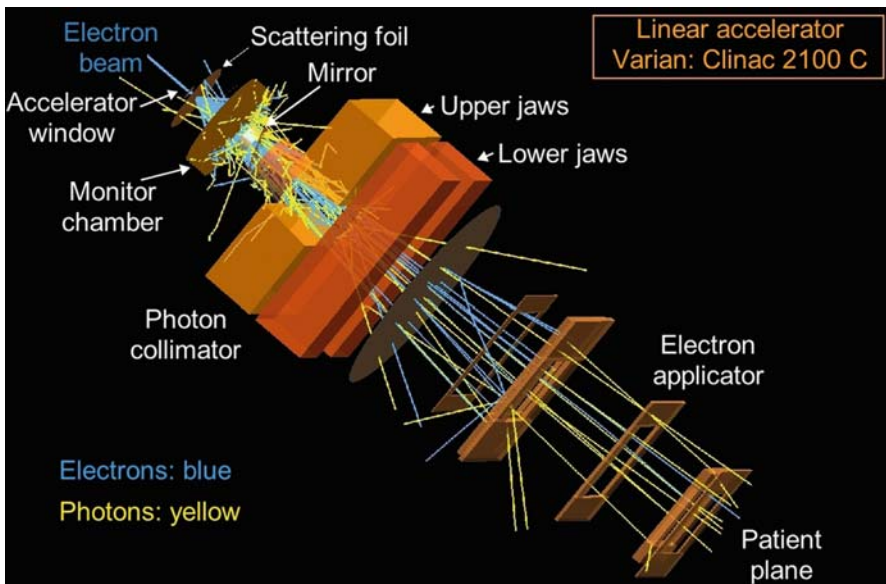


## Coulomb Scattering

This chapter deals with various types of elastic scattering interactions that heavy and light charged particles can have with atoms of an absorber. The interactions fall into the general category of Coulomb interactions and the chapter starts with a discussion of the intriguing Geiger-Marsden experiment of alpha particle scattering on thin gold foils. The experiment is of great historical importance and its results have led to Rutherford's ingenious conclusion that most of the atom is empty space and that most of the atomic mass is concentrated in the atomic nucleus. The kinematics of the  $\alpha$  particle scattering is discussed in detail and the differential and total cross section concept for scattering is introduced for Rutherford scattering and expanded to other types of Coulomb scattering.



The chapter continues with a discussion of the Mott electron-nucleus scattering and introduces correction factors for electron spin, nuclear recoil, and the finite size of the nucleus to achieve better agreement with measured data. A brief discussion of the form factor representing the Fourier transform of the nuclear charge density follows and the chapter continues with a general discussion of elastic scattering of charged particles. The chapter concludes with a discussion of the characteristic scattering distance, scattering cross section and mean square scattering angle for various scattering events occurring on single scattering centers (single scattering) as well as the mean square scattering angle and mass scattering power for multiple scattering.

## 2.1 General Aspects of Coulomb Scattering

Coulomb scattering is a general term used to describe elastic Coulomb interactions between two charged particles: an energetic projectile and a target. Much of the knowledge in atomic, nuclear, and particle physics has been derived from various Coulomb scattering experiments, starting with the famous Geiger and Marsden experiment of 1909 in which  $\alpha$  particles were scattered on gold nuclei. Based on the angular distribution of the scattered  $\alpha$  particles, measured by Geiger and Marsden, Rutherford concluded that most of the atomic mass and the positive atomic charge are concentrated in the atomic nucleus which is at least four orders of magnitude smaller than the size of the atom.

The Rutherford model of the atom revolutionized physics in particular and science in general. Since then other Coulomb-type scattering experiments were carried out, typically using energetic protons or electrons as projectiles bombarding atomic nuclei or orbital electrons with the objective to learn more about the atomic and nuclear structure.

It is now well understood that in order for a particle to be useful as a nuclear probe, its de Broglie wavelength (Sect. 1.22.1) must be of the order of the nuclear size which is currently estimated with the relationship  $R = R_0 \sqrt[3]{A}$  given in (1.26) with  $R$  the nuclear radius,  $A$  the atomic mass number and  $R_0$  the nuclear radius constant (1.25 fm). As shown in Sect. 1.22.1, the de Broglie wavelength of a particle can be expressed as a function of the particle's kinetic energy  $E_K$  as

$$\lambda = \frac{2\pi\hbar c}{E_K \sqrt{1 + \frac{2E_0}{E_K}}} \begin{cases} \approx \frac{2\pi\hbar c}{\sqrt{2E_0 E_K}} & \text{for } E_K \ll E_0 = m_0 c^2, \\ \approx \frac{2\pi\hbar c}{E_K} \approx \frac{2\pi\hbar c}{E} & \text{for } E_K \gg E_0 = m_0 c^2. \end{cases} \quad (2.1)$$

In Fig. 1.6 we show the de Broglie wavelength  $\lambda$  against kinetic energy  $E_K$  for electrons, protons, and  $\alpha$  particles. Typical nuclear size is of the order of 10 fm and the de Broglie wavelength  $\lambda$  of 10 fm is attained at kinetic energies  $E_K$  of 2 MeV for  $\alpha$  particles, 10 MeV for protons, and 130 MeV for electrons. Electrons with kinetic energies above 200 MeV can serve as an

excellent probe for nuclear studies, not only because these electrons possess a suitable de Broglie wavelength but also because they are point-like and experience only Coulomb interactions with the nuclear constituents even when they penetrate the nucleus. This is in contrast to heavy charged particles which upon penetration of the nucleus will undergo strong interactions in addition to Coulomb interactions, making the analysis of experimental results difficult and cumbersome.

In the first approximation electron scattering on a nucleus can be treated like Rutherford scattering; however, when doing so, several other interactions are ignored, such as: spin effects in magnetic interactions; energy transfer to the nucleus of the scatterer (target recoil); relativistic and quantum effects; and effects of the finite size of the nucleus. Modern scattering theories now account for these additional interactions; however, they are still based on principles enunciated 100 years ago in Manchester by Geiger, Marsden, and Rutherford.

Scattering of  $\alpha$  particles on atomic nuclei is referred to as Rutherford scattering in honor of Rutherford's contribution to the understanding of the scattering process as well as the structure of the atom. In addition to the Rutherford scattering of  $\alpha$  particles on atomic nuclei (see Sect. 2.2), the most notable other Coulomb elastic scattering phenomena are:

- Scattering of energetic electrons on atomic nuclei referred to as Mott scattering (Sect. 2.5).
- Scattering of electrons on atomic orbital electrons referred to as Møller scattering.
- Scattering of positrons on atomic orbital electrons referred to as Bhabha scattering.
- Multiple scattering involving any one of the above listed scattering types and referred to as Molière multiple scattering (Sect. 2.7).

## 2.2 Geiger–Marsden Experiment

In 1909 *Hans Geiger* and *Ernest Marsden* in collaboration with *Ernest Rutherford* carried out an experiment studying the scattering of 5.5 MeV  $\alpha$  particles on a thin gold foil with a thickness of the order of  $10^{-6}$  m. They obtained the  $\alpha$  particles from radon-222, a natural  $\alpha$ -particle emitter, collimated them into a small pencil beam, and directed the beam in vacuum onto a thin gold foil in which scattering occurred. The scattered  $\alpha$  particles were detected by counting with a low-power microscope the scintillations produced in a zinc sulphide (ZnS) receptor (area:  $1 \text{ cm}^2$ ) that could be rotated around the foil at a given distance from the source. The alpha particle counter was invented several years before by *William Crookes* and called the spintharoscope. The Geiger–Marsden experiment, shown schematically in Fig. 2.1, seems rather mundane; however, its peculiar and unexpected results had a profound effect on modern physics in particular and on humanity in general.

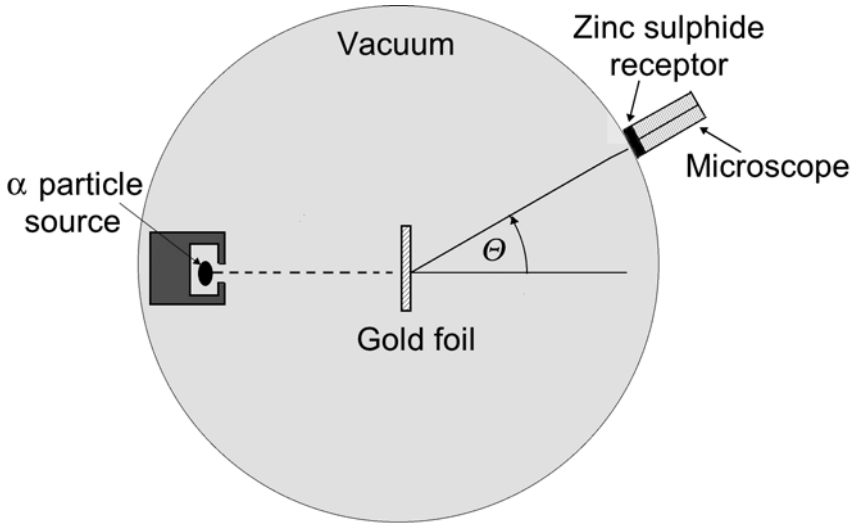


**Fig. 2.1.** Schematic diagram of the Geiger–Marsden experiment in the study of  $\alpha$ -particle scattering on gold nuclei in a thin gold foil.  $\theta$  is the total scattering angle for  $\alpha$  particles upon traversing the  $1\ \mu\text{m}$  thick gold foil and undergoing a large number of scattering interactions

### 2.2.1 Thomson Model of the Atom

In 1898 *Joseph J. Thomson*, who is also credited with the discovery of the electron in 1897, proposed an atomic model in which the mass of the atom is distributed uniformly over the volume of the atom with a radius of the order of  $1\ \text{Å}$  and negatively charged electrons are dispersed uniformly within a continuous spherical distribution of positive charge. The electrons form rings and each ring can accommodate a certain upper limit in the number of electrons and then other rings begin to form. With this ring structure Thomson could in principle account for the periodicity of chemical properties of elements. A schematic representation of the Thomson’s atomic model, often referred to as the “*plum-pudding model*”, is given in Fig. 2.2a, suggesting the following features:

- In the ground state of the atom the electrons are fixed at their equilibrium positions and emit no radiation.
- In an excited state of the atom the electrons oscillate about their equilibrium positions and emit radiation through dipole oscillations by virtue of possessing charge and being continuously accelerated or decelerated (Larmor relationship).

According to the Thomson atomic model the angular distribution of a pencil beam of  $\alpha$  particles scattered in the gold foil in the Geiger–Marsden experiment is Gaussian and given by the following expression (for derivation see Sect. 2.7.5)

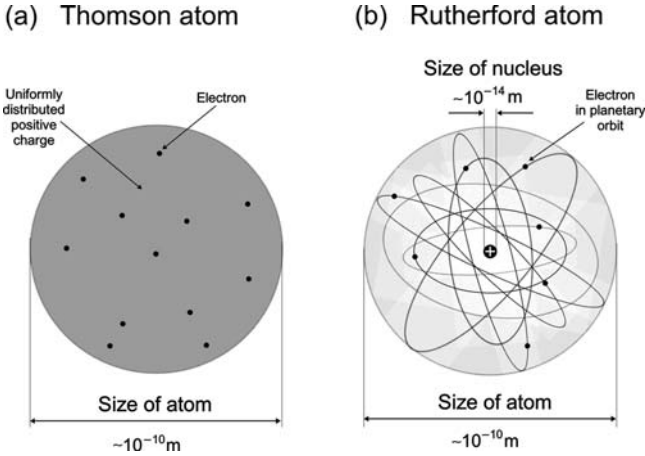


**Fig. 2.2.** Schematic diagram of two atomic models: (a) Thomson “plum-pudding” model of 1898 in which the electrons are uniformly distributed in a sea of positive atomic charge and (b) Rutherford nuclear model in which the electrons revolve in empty space around the nucleus that is positively charged and contains most of the atomic mass. The size of the nucleus with diameter of the order of  $10^{-14}$  m is at least 4 orders of magnitude smaller than the size of the Rutherford atom with diameter of the order of  $10^{-10}$  m. The size of the Thomson atom is of the order of  $10^{-10}$  m, similar to the size of Rutherford atom

$$N(\theta)d\theta = \frac{2\theta N_0}{\overline{\theta^2}} e^{-\frac{\theta^2}{\overline{\theta^2}}} d\theta, \tag{2.2}$$

where

- $\theta$  is the scattering angle of the  $\alpha$  particle after it passes through the gold foil (note: the  $\alpha$  particle undergoes  $\sim 10^4$  interactions as a result of a foil thickness of  $10^{-6}$  m and an approximate atomic diameter of  $10^{-10}$  m.
- $N(\theta) d\theta$  is the number of  $\alpha$  particles scattered within the angular range of  $\theta$  to  $\theta+d\theta$ .
- $N_0$  is the number of  $\alpha$  particles striking the gold foil.
- $\overline{\theta^2}$  is the mean square net deflection experimentally determined to be of the order of  $3 \times 10^{-4}$  rad<sup>2</sup>, i.e.,  $\sqrt{\overline{\theta^2}} \approx 1^\circ$ .

Geiger and Marsden found that more than 99 % of the  $\alpha$  particles incident on the gold foil were scattered at angles less than  $3^\circ$  and that their distribution followed a Gaussian shape given in (2.2); however, they also found that one in  $\sim 10^4$   $\alpha$  particles was scattered with a scattering angle  $\theta$  exceeding  $90^\circ$ . This implied a measured probability of  $10^{-4}$  for scattering with scattering angle  $\theta > 90^\circ$ , in drastic disagreement with the probability of  $10^{-3500}$  predicted by the theory based on the Thomson atomic model, as shown in (2.3) below.

According to the Thomson atomic model the probability for  $\alpha$ -particle scattering with  $\Theta > 90^\circ$  (i.e., with a scattering angle  $\Theta$  between  $\frac{1}{2}\pi$  and  $\pi$ ) is calculated by integrating (2.2) from  $\frac{1}{2}\pi$  to  $\pi$  as follows

$$\begin{aligned} \frac{N\left(\Theta > \frac{\pi}{2}\right)}{N_0} &= \frac{\int_{\pi/2}^{\pi} N(\Theta) d\Theta}{N_0} = - \int_{\frac{\pi}{2}}^{\pi} e^{-\frac{\Theta^2}{\Theta^2}} d\left(-\frac{\Theta^2}{\Theta^2}\right) \\ &= - e^{-\frac{\Theta^2}{\Theta^2}} \Big|_{\frac{\pi}{2}}^{\pi} = -e^{-\left\{\frac{180^\circ}{1^\circ}\right\}^2} + e^{-\left\{\frac{90^\circ}{1^\circ}\right\}^2} = e^{-90^2} \approx 10^{-3500}, \end{aligned} \quad (2.3)$$

where we use the experimentally determined value of  $1^\circ$  for the root mean square angle  $\sqrt{\overline{\Theta^2}}$ .

## 2.2.2 Rutherford Model of the Atom

At the time of the Geiger–Marsden experiment, the Thomson atomic model was the prevailing atomic model based on the assumption that the positive charges and the negative (electron) charges of an atom were distributed uniformly over the atomic volume (“plum-pudding” model) to make the atom neutral on the outside. The theoretical result of  $10^{-3500}$  for the probability of  $\alpha$ -particle scattering with a scattering angle greater than  $90^\circ$  on a gold foil consisting of Thomson atoms is an extremely small number in comparison with the result of  $10^{-4}$  obtained experimentally by Geiger and Marsden. This discrepancy between experiment and theory highlighted a serious problem with the Thomson atomic model and stimulated *Ernest Rutherford* to propose a completely new atomic model that agreed better with experimental results obtained by Geiger and Marsden. The two main features of the Rutherford model are as follows:

1. Mass and positive charge of the atom are concentrated in the nucleus the size of which is of the order of  $10^{-15}$  m = 1 fm.
2. Negatively charged electrons revolve about the nucleus in a cloud, the radius of which is of the order of  $10^{-10}$  m = 1 Å.

The two competing atomic models are depicted schematically in Fig. 2.2. Contrary to the Thomson “plum-pudding” atomic model, essentially all mass of the Rutherford atom is concentrated in the atomic nucleus that is also the seat of the positive charge of the atom and has a radius of the order of  $10^{-15}$  m, as shown schematically in Fig. 2.2b. As shown in (1.27), the density of the nucleus with mass  $M$  is enormous with an order of magnitude of  $1.5 \times 10^{14}$  g · cm<sup>-3</sup>.

As for the atomic electrons, Rutherford proposed that they are distributed in a spherical cloud on the periphery of the atom with a radius of the order of  $10^{-10}$  m; however, he did not speculate on the rules governing the motion of electrons in an atom. It was *Niels Bohr* who soon thereafter expanded the Rutherford model by proposing four postulates, one of them dealing with quantization of electron angular momentum, which allowed him to derive from first principles the electron planetary motion in one-electron structures (See Sect. 3.1). Rutherford, a superb experimental physicist, and Bohr, an extremely gifted theoretical physicist, are credited with developing the currently accepted atomic model which in their honor is referred to as the Rutherford–Bohr atomic model.

## 2.3 Rutherford Scattering

### 2.3.1 Kinematics of Rutherford Scattering

Based on his model and five additional assumptions, Rutherford derived the kinematics for the scattering of  $\alpha$  particles on gold nuclei using basic principles of classical mechanics. The five additional assumptions are as follows:

1. Scattering of  $\alpha$  particles on gold nuclei is elastic.
2. The mass of the gold nucleus  $M$  is much larger than the mass of the  $\alpha$  particle  $m_\alpha$ , i.e.,  $M \gg m_\alpha$ .
3. Scattering of  $\alpha$  particles on atomic electrons is negligible because  $m_\alpha \gg m_e$ , where  $m_e$  is the electron mass.
4. The  $\alpha$  particle does not penetrate the nucleus (no nuclear reactions).
5. The classical relationship for the kinetic energy  $E_K$  of the  $\alpha$  particle, i.e.,  $E_K = \frac{1}{2}m_\alpha v_\alpha^2$ , is valid, where  $v_\alpha$  is the velocity of the  $\alpha$  particle.

Rutherford used concepts of classical mechanics in his derivation of the kinematics of  $\alpha$ -particle scattering. To show that this was an acceptable approach we determine the speed of 5.5 MeV  $\alpha$  particles used in the Geiger–Marsden experiment. The speed  $v_\alpha$  of the  $\alpha$  particles relative to the speed of light in vacuum  $c$  for 5.5 MeV  $\alpha$  particles can be calculated using either the classical relationship or the relativistic relationship of (1.58). Note that  $m_\alpha c^2 = 3727$  MeV:

1. The *classical calculation* is done using the classical expression for the kinetic energy  $E_K$  of the  $\alpha$  particle

$$E_K = \frac{1}{2}m_\alpha v_\alpha^2 = \frac{1}{2}m_\alpha c^2 \left\{ \frac{v_\alpha^2}{c^2} \right\}. \quad (2.4)$$

Solve (2.4) for  $v_\alpha/c$  to obtain

$$\frac{v_\alpha}{c} = \sqrt{\frac{2E_K}{m_\alpha c^2}} = \sqrt{\frac{2 \times 5.5 \text{ MeV}}{3727 \text{ MeV}}} = 0.0543. \quad (2.5)$$

2. The *relativistic calculation* is carried out using the relativistic expression (1.68) for the kinetic energy  $E_K$  of the  $\alpha$  particle

$$E_K = \frac{m_\alpha c^2}{\sqrt{1 - \left(\frac{v_\alpha}{c}\right)^2}} - m_\alpha c^2. \quad (2.6)$$

Solve (2.6) for  $v_\alpha/c$  to obtain

$$\frac{v_\alpha}{c} = \sqrt{1 - \frac{1}{\left(1 + \frac{E_K}{m_\alpha c^2}\right)^2}} = \sqrt{1 - \frac{1}{\left(1 + \frac{5.5}{3727}\right)^2}} = 0.0543 \quad (2.7)$$

The relativistic calculation of (2.6) and classical calculation of (2.4) give identical results since the velocity of the  $\alpha$  particle is much smaller than  $c$ , the speed of light in vacuum, or  $(v_\alpha/c) \ll 1$ , for  $\alpha$  particles with kinetic energy  $E_K$  of the order of a few million electron volts. Rutherford's use of the simple classical relationship rather than the correct relativistic expression for the kinetic energy of the naturally occurring  $\alpha$  particles was thus justified. Note that all naturally occurring  $\alpha$  particles have kinetic energy of the order of a few million electron volts, so the use of classical mechanics is appropriate for all naturally occurring  $\alpha$  particles.

The interaction between the  $\alpha$  particle (charge  $ze$ ) and the nucleus (charge  $Ze$ ) is a repulsive Coulomb interaction between two positive point charges, and, as result, the  $\alpha$  particle follows a hyperbolic trajectory, as shown schematically in Fig. 2.3. Note that  $\theta$  represents the scattering angle in a single  $\alpha$ -particle interaction with one nucleus, whereas  $\Theta$  of (2.2) represents the scattering angle resulting from the  $\alpha$  particle traversing the thin gold foil and undergoing some  $10^4$  interactions while traversing the foil.

For a single  $\alpha$ -particle interaction depicted in Fig. 2.3 the nucleus is in the outer focus of the hyperbola because of the repulsive interaction between the  $\alpha$  particle and the nucleus. For an interaction between two charges of opposite sign (for example, energetic electron interacting with atomic nucleus) the Coulomb interaction is attractive and the trajectory of the projectile is also a hyperbola but the target resides in the inner focus of the hyperbola.

Two important parameters of Coulomb scattering are the impact parameter  $b$  and the scattering angle  $\theta$ . As shown in Fig. 2.3:

- Impact parameter  $b$  is defined as the perpendicular distance between the initial velocity vector  $\mathbf{v}_i$  of the projectile and the center of the target it is approaching.
- Scattering angle  $\theta$  is defined as the angle between the initial momentum vector  $\mathbf{p}_i$  and the final momentum vector  $\mathbf{p}_f$ .

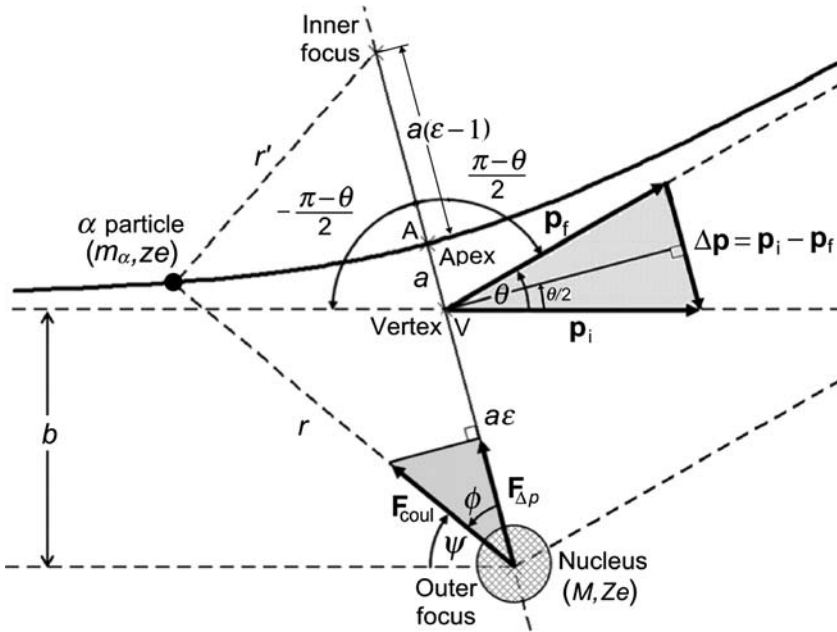


**Fig. 2.3.** Schematic diagram for scattering of an  $\alpha$  particle on a nucleus:  $\theta$  is the scattering angle;  $b$  the impact parameter;  $\Delta \mathbf{p}$  the change in  $\alpha$ -particle momentum;  $v_i$  the initial velocity of the  $\alpha$  particle; and  $\mathbf{p}_i$  the initial momentum of the  $\alpha$  particle. The trajectory of the  $\alpha$  particle is a hyperbola as result of the repulsive Coulomb interaction between the  $\alpha$  particle and the nucleus. The nucleus is in the outer focus of the hyperbolic trajectory of the  $\alpha$  particle

### 2.3.2 Distance of Closest Approach in Head-on Collision Between $\alpha$ -Particle and Nucleus

A special case of Rutherford scattering occurs when  $b = 0$  corresponding to the  $\alpha$  particle being on a direct-hit trajectory. Considering the classical conservation of energy in a direct hit  $\alpha$ -particle elastic scattering event, the following points can be made:

1. The total energy  $E(r)$  of the  $\alpha$  particle–nucleus system consists of two components: kinetic energy  $E_K(r)$  of the  $\alpha$  particle and the repulsive Coulomb potential energy  $E_P(r)$  where

$$E_K(r) = \frac{m_\alpha v^2}{2}, \tag{2.8}$$

$$E_P(r) = \frac{zZe^2}{4\pi\epsilon_0} \frac{1}{r}. \tag{2.9}$$

and  $r$  is the distance between the  $\alpha$  particle and the nucleus.

2. The scattering is elastic. The kinetic energy  $E_K$  of the  $\alpha$  particle does not remain constant during the scattering process; however, the initial kinetic energy  $(E_K)_i$  is equal to the final kinetic energy  $(E_K)_f$  since the nucleus is assumed to remain stationary. This means that the final velocity of the  $\alpha$  particle  $v_f$  is equal to the initial velocity of the  $\alpha$  particle  $v_i$ .
3. In general, total energy  $E(r)$  is the sum of the kinetic energy  $E_K(r)$  and potential energy  $E_P(r)$

$$E(r) = (E_K)_i = E_K(r) + E_P(r) = E_K(r) + \frac{zZe^2}{4\pi\epsilon_0} \frac{1}{r}. \quad (2.10)$$

4. The total energy  $E(r)$  at any distance  $r > D_{\alpha-N}$  from the nucleus equals the initial kinetic energy  $(E_K)_i$  of the  $\alpha$  particle, since  $E_P(r = \infty) \rightarrow 0$ . As the  $\alpha$  particle approaches the nucleus, its velocity  $v_\alpha$  and kinetic energy  $E_K(r)$  diminish and the repulsive potential energy  $E_P(r)$  increases with the sum of the two always equal to the initial kinetic energy  $(E_K)_i$  of the  $\alpha$  particle.
5. In its approach toward the nucleus the  $\alpha$  particle eventually stops at a distance from the nucleus  $D_{\alpha-N}$ , defined as the distance of closest approach. At  $r = D_{\alpha-N}$  the  $\alpha$  particle kinetic energy  $E_K(r = D_{\alpha-N})$  is zero, and the total energy  $E(r)$  equals the potential energy  $E_P(r = D_{\alpha-N})$  which is expressed as

$$\begin{aligned} E(r = D_{\alpha-N}) &= (E_K)_i = E_K(r = D_{\alpha-N}) + E_P(r = D_{\alpha-N}) \\ &= 0 + \frac{zZe^2}{4\pi\epsilon_0} \frac{1}{D_{\alpha-N}}. \end{aligned} \quad (2.11)$$

The distance of closest approach  $D_{\alpha-N}$  between the  $\alpha$  particle with  $(E_K)_i = 5.5$  MeV and a gold nucleus ( $Z = 79$ ) in a direct hit scattering event is determined from (2.11) as follows

$$D_{\alpha-N} = \frac{zZe^2}{4\pi\epsilon_0} \frac{1}{E_K} = \frac{2 \times 79 \times e \times 1.6 \times 10^{-19} \text{ C} \cdot \text{V} \cdot \text{m}}{4\pi \times 8.85 \times 10^{-12} \text{ C} \times 5.5 \times 10^6 \text{ eV}} = 41.3 \text{ fm} \quad (2.12)$$

or

$$D_{\alpha-N} = \frac{zZ\hbar c\alpha}{E_K} = \frac{2 \times 79 \times 197.3 \text{ MeV} \cdot \text{fm}}{137 \times 5.5 \text{ MeV}} \approx 41.3 \text{ fm}$$

For naturally occurring  $\alpha$  particles interacting with nuclei of atoms the distance of closest approach  $D_{\alpha-N}$  exceeds the radius  $R$  of the nucleus. Thus, the  $\alpha$  particle does not penetrate the nucleus and no nuclear reaction occurs. For example, as shown in (2.12),  $D_{\alpha-N}$  for the Geiger–Marsden experiment with 5.5 MeV  $\alpha$ -particle scattering on gold nuclei is 41.3 fm compared to the gold nucleus radius determined from (1.26) as

$$R = R_0 \sqrt[3]{A} = 1.25 \text{ fm } \sqrt[3]{197} \approx 7.3 \text{ fm}, \quad (2.13)$$

where  $R_0$  is the nuclear radius constant equal to 1.25 fm, as discussed in Sect. 1.16.1.

### 2.3.3 General Relationship between Impact Parameter and Scattering Angle

The general relationship between the impact parameter  $b$  and the scattering angle  $\theta$  may be derived most elegantly by determining two independent expressions for the change in momentum  $\Delta p$  of the scattered  $\alpha$  particle. The momentum transfer is along the symmetry line that bisects the angle  $\pi - \theta$ , as indicated in Fig. 2.3. The magnitude of the repulsive Coulomb force  $F_{\text{Coul}}$  acting on the  $\alpha$  particle is given by

$$F_{\text{Coul}} = \frac{zZe^2}{4\pi\epsilon_0} \frac{1}{r^2}, \quad (2.14)$$

where

- $r$  is the distance between the  $\alpha$  particle and the nucleus  $M$ ,
- $z$  is the atomic number of the  $\alpha$  particle (for helium  $z = 2$  and  $A = 4$ ),
- $Z$  is the atomic number of the absorber (for gold  $Z = 79$  and  $A = 197$ ).

Since the component of the force  $F_{\text{Coul}}$  in the direction of the momentum transfer is  $F_{\Delta p} = F_{\text{Coul}} \cos \phi$ , the momentum transfer (impulse of force)  $\Delta p$  may be written as the time integral of the force component  $F_{\Delta p}$  as follows

$$\begin{aligned} \Delta p &= \int_{-\infty}^{\infty} F_{\Delta p} dt = \int_{-\infty}^{\infty} F_{\text{Coul}} \cos \phi dt = \frac{zZe^2}{4\pi\epsilon_0} \int_{-\frac{\pi-\theta}{2}}^{\frac{\pi-\theta}{2}} \frac{\cos \phi}{r^2} \frac{dt}{d\phi} d\phi \\ &= \frac{zZe^2}{4\pi\epsilon_0} \int_{-\frac{\pi-\theta}{2}}^{\frac{\pi-\theta}{2}} \frac{\cos \phi}{\omega r^2} d\phi, \end{aligned} \quad (2.15)$$

where

- $\phi$  is the angle between the radius vector  $r$  and the bisector, as also shown in Fig. 2.3,
- $\frac{dt}{d\phi}$  is the inverse of the angular frequency  $\omega$ .

The angular frequency  $\omega = d\phi/dt = v/r$  can be expressed as a function of the impact parameter  $b$ , initial  $\alpha$ -particle velocity  $v_i$ , and radius vector  $r$  by invoking conservation of angular momentum  $\mathbf{L}$ , where  $\mathbf{L}$  is in general defined as

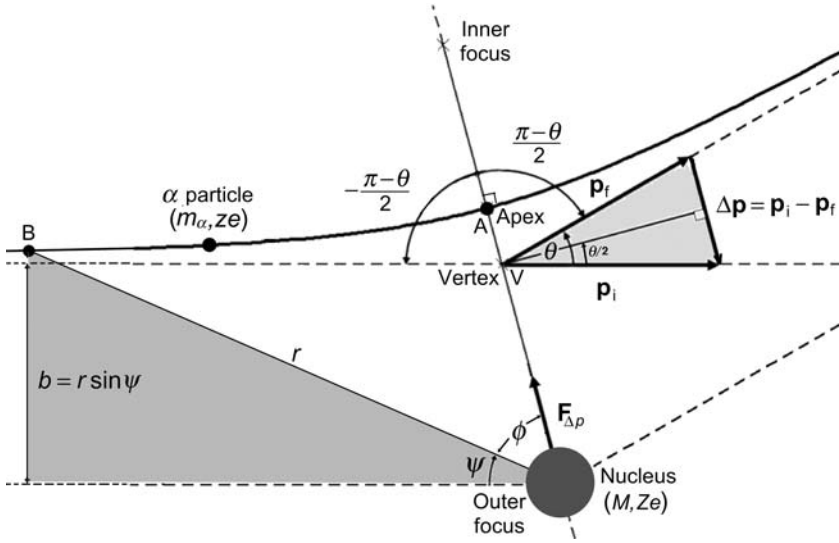


**Fig. 2.4.** Geometry for determination of the angular momentum  $\mathbf{L}$  for two different points on the  $\alpha$ -particle trajectory. Point A is for the  $\alpha$  particle located in the apex of the hyperbola and point B is for the  $\alpha$  particle located at a very large distance from the nucleus

$$\mathbf{L} = \mathbf{r} \times \mathbf{p} = \mathbf{r} \times m_\alpha \mathbf{v}. \quad (2.16)$$

With the help of Fig.2.4 we now express  $|\mathbf{L}| = L$ , the magnitude of the angular momentum  $\mathbf{L}$ , for two different points (A and B) on the  $\alpha$ -particle hyperbolic trajectory. Point A is at the apex of the hyperbola and point B is at a very large distance from the nucleus where the  $\alpha$ -particle position defines the impact parameter  $b$ . The angular momentum  $L$  at point B is given as

$$|\mathbf{L}| = L = r m_\alpha v_i \sin \psi = m_\alpha v_i b, \quad (2.17)$$

while for the apex point A, where  $\mathbf{v}$  and  $\mathbf{r}$  are perpendicular to each other and  $v = \omega r$ , it is

$$|\mathbf{L}| = L = |\mathbf{r} \times m_\alpha \mathbf{v}| = m_\alpha r v \sin 90^\circ = m_\alpha \omega r^2. \quad (2.18)$$

Using the conservation of angular momentum  $L$ , we merge (2.17) and (2.18) to get

$$L = m_\alpha v_i b = m_\alpha \omega r^2, \quad (2.19)$$

and the following expression for the angular frequency  $\omega$

$$\omega = \frac{v_i b}{r^2}, \quad (2.20)$$

with  $v_i$  the initial velocity of the  $\alpha$  particle at  $r = \infty$ . Since the scattering is elastic, the kinetic energy will be conserved in the scattering interaction, so it follows that the final  $\alpha$  particle velocity  $v_f$  will be equal to the initial  $\alpha$  particle velocity ( $v_f = v_i$ ).

After inserting (2.20) into (2.15) we get a simple integral for  $\Delta p$  with the following solution

$$\Delta p = \frac{zZe^2}{4\pi\epsilon_0} \frac{1}{v_i b} \int_{-\frac{\pi-\theta}{2}}^{\frac{\pi-\theta}{2}} \cos \phi \, d\phi = \frac{zZe^2}{4\pi\epsilon_0} \frac{1}{v_\infty b} \left\{ \sin \phi \right\}_{-\frac{\pi-\theta}{2}}^{+\frac{\pi-\theta}{2}} = 2 \frac{zZe^2}{4\pi\epsilon_0} \frac{1}{v_i b} \cos \frac{\theta}{2}. \quad (2.21)$$

With the help of the momentum vector diagram, given in Figs. 2.3 and 2.4, the momentum transfer  $\Delta p$  may also be written as

$$\Delta p = 2p_i \sin \frac{\theta}{2} = 2m_\alpha v_i \sin \frac{\theta}{2}. \quad (2.22)$$

Combining (2.21) and (2.22) we obtain the following expressions for the impact parameter  $b$

$$\begin{aligned} b &= \frac{zZe^2}{4\pi\epsilon_0 m_\alpha v_i^2} \cot \frac{\theta}{2} = \frac{1}{2} \frac{zZe^2}{4\pi\epsilon_0} \frac{1}{E_K} \cot \frac{\theta}{2} \\ &= \frac{1}{2} D_{\alpha-N} \cot \frac{\theta}{2} = \frac{1}{2} D_{\alpha-N} \sqrt{\frac{1 + \cos \theta}{1 - \cos \theta}}, \end{aligned} \quad (2.23)$$

with the use of:

1. Classical relationship for the kinetic energy of the  $\alpha$  particle ( $E_K = \frac{1}{2} m_\alpha v_i^2$ ), since  $v_i \ll c$ .
2. Definition of  $D_{\alpha-N}$  as the distance of closest approach between the  $\alpha$  particle and the nucleus in a “direct-hit” head-on collision for which the impact parameter  $b = 0$ , the scattering angle  $\theta = \pi$ , and  $D_{\alpha-N} = zZe^2 / (4\pi\epsilon_0 E_K)$  from (2.12).

### 2.3.4 Hyperbolic Trajectory and Distance of Closest Approach

Equations for the hyperbolic trajectory of an alpha particle interacting with a nucleus can be derived from the diagram given in Fig. 2.3 and the simple rule governing the hyperbola with the target in the outer focus because of the repulsive interaction between the projectile ( $\alpha$  particle) and the target (nucleus)

$$r - r' = 2a, \quad (2.24)$$

where

- $a$  is the distance between the apex and the vertex of the hyperbola,
- $r$  is the distance between the point of interest on the hyperbola and the outer focus,
- $r'$  is the distance between the point of interest on the hyperbola and the inner focus.

The parameters of the hyperbola, such as  $a$ ,  $r$ , and  $r'$ , are defined in Fig. 2.3 and the locations of the inner focus, outer focus, apex A and vertex V are also indicated in Fig. 2.3. Solving (2.24) for  $r'$  and squaring the result, we get the following expression for  $(r')^2$

$$(r')^2 = r^2 - 4ar + 4a^2. \quad (2.25)$$

Using the law of cosines in conjunction with Fig. 2.3, we express  $(r')^2$  as

$$(r')^2 = r^2 - 4a\varepsilon r \cos \phi + 4a^2\varepsilon^2, \quad (2.26)$$

where  $\varepsilon$  is the eccentricity of the hyperbola.

Subtracting (2.26) from (2.25) and solving for  $r(\phi)$ , we now obtain the following general equation for the hyperbolic trajectory of the  $\alpha$  particle

$$r(\phi) = \frac{a(\varepsilon^2 - 1)}{\varepsilon \cos \phi - 1}. \quad (2.27)$$

Three separate special conditions are of interest with regard to (2.27):

1.  $r = \infty$  for determining the eccentricity  $\varepsilon$ .
2.  $\phi = 0$  for determining the general distance of closest approach  $R_{\alpha-N}$ .
3.  $\theta = \pi$  for determining the distance of closest approach in a direct hit that results in the shortest distance of closest approach defined as  $D_{\alpha-N}$  in (2.12).

**Eccentricity**  $\varepsilon$  is determined as follows:

For  $r = \infty$  the angle  $\phi$  equals to  $\frac{1}{2}(\pi - \theta)$  and, to get  $r = \infty$ , the denominator in (2.27)  $[\varepsilon \cos[\frac{1}{2}(\pi - \theta)] - 1]$  must equal to zero, resulting in the following relationship for the eccentricity  $\varepsilon$

$$\varepsilon \cos \frac{\pi - \theta}{2} - 1 = \varepsilon \sin \frac{\theta}{2} - 1 = 0 \quad \text{or} \quad \varepsilon = \frac{1}{\sin \frac{\theta}{2}}. \quad (2.28)$$

**Distance of closest approach**  $R_{\alpha-N}$  between the  $\alpha$  particle and the nucleus in a non-direct hit collision ( $\theta < \pi$  and  $\phi = 0$ ) is from (2.27) given as

$$R_{\alpha-N} = r(\phi = 0) = \frac{a(\varepsilon^2 - 1)}{\varepsilon - 1} = a(1 + \varepsilon) = a \left\{ 1 + \frac{1}{\sin \frac{\theta}{2}} \right\}. \quad (2.29)$$

The result  $R_{\alpha-N} = a(1 + \varepsilon)$  can also be obtained directly from Fig. 2.3 by recognizing that the distance between the outer focus and apex of the hyperbola equals to  $(a\varepsilon + a)$ .

**Distance of closest approach in a direct-hit collision**,  $D_{\alpha-N}$  ( $b = 0$ ;  $\theta = \pi$ ) can now from (2.29) with  $\theta = \pi$  be written as

$$D_{\alpha-N} = R_{\alpha-N}(\theta = \pi) = 2a, \quad (2.30)$$

from where it follows that  $a$ , the distance between the apex A and the vertex V of the hyperbola, (see Figs. 2.3 and 2.4) is equal to  $\frac{1}{2}D_{\alpha-N}$ . This allows us to express  $R_{\alpha-N}$  of (2.29) as a function of the direct-hit distance of closest approach  $D_{\alpha-N}$  or as a function of the impact parameter  $b$  using the relationship (2.23) between  $D_{\alpha-N}$  and  $b$

$$R_{\alpha-N} = a \left\{ 1 + \frac{1}{\sin \frac{\theta}{2}} \right\} = \frac{D_{\alpha-N}}{2} \left\{ 1 + \frac{1}{\sin \frac{\theta}{2}} \right\} = b \frac{1 + \sin \frac{\theta}{2}}{\cos \frac{\theta}{2}} = b \frac{\cos \frac{\theta}{2}}{1 - \sin \frac{\theta}{2}}. \quad (2.31)$$

### 2.3.5 Hyperbola in Polar Coordinates

In *polar coordinates*  $(r, \varphi)$  the hyperbolic  $\alpha$ -particle trajectory may be expressed as

$$\frac{1}{r} = \frac{1}{b} \sin \psi + \frac{a}{b^2} (\cos \psi - 1), \quad (2.32)$$

with parameters  $a$ ,  $b$ , and  $\psi$  defined in Fig. 2.3. Note that  $\psi$  and  $\phi$  are different angles and that the following relationship for angles  $\psi$ ,  $\phi$ , and  $\theta$  applies

$$\psi + \phi = \left| \frac{\pi - \theta}{2} \right|. \quad (2.33)$$

It can be shown that the general expressions (2.32) and (2.27) defining the hyperbola are equivalent.

## 2.4 Cross Sections for Rutherford Scattering

### 2.4.1 Differential Cross-Section for Rutherford Scattering: Classical Derivation

The differential cross section  $d\sigma_{\text{Ruth}}/d\Omega$  for Rutherford scattering into a solid angle  $d\Omega = 2\pi \sin \theta d\theta$  that corresponds to an angular aperture between  $\theta$  and  $\theta + d\theta$  (equivalent to impact parameters between  $b$  and  $b - db$ ), assuming the azimuthal distribution to be isotropic, is the area of a ring with mean radius  $b$  and width  $db$

$$d\sigma_{\text{Ruth}} = 2\pi b \, db = 2\pi \frac{b}{\sin \theta} \sin \theta \left| \frac{db}{d\theta} \right| d\theta. \quad (2.34)$$

Recognizing that

$$d\Omega = 2\pi \sin \theta \, d\theta, \quad (2.35)$$

expressing  $\sin \theta$  as

$$\sin \theta = 2 \sin \frac{\theta}{2} \cos \frac{\theta}{2}, \quad (2.36)$$

and, using (2.23) for the impact parameter  $b$  to determine  $|db/d\theta|$  as

$$\left| \frac{db}{d\theta} \right| = \frac{D_{\alpha-N}}{4} \frac{1}{\sin^2 \frac{\theta}{2}}, \quad (2.37)$$

we obtain from (2.34) combined with (2.35), (2.36), and (2.37) the following expression for  $d\sigma_{\text{Ruth}}/d\Omega$ , the differential Rutherford cross section

$$\frac{d\sigma_{\text{Ruth}}}{d\Omega} = \left( \frac{D_{\alpha-N}}{4} \right)^2 \frac{1}{\sin^4 \frac{\theta}{2}} = \left( \frac{D_{\alpha-N}}{4} \right)^2 \frac{1}{(1 - \cos \theta)^2}. \quad (2.38)$$

Inserting the expression for  $D_{\alpha-N}$  of (2.12) into (2.38) and using the definition of the fine structure constant  $\alpha = e^2 (4\pi\epsilon_0 \hbar c)^{-1}$ , we can express the Rutherford differential cross section as

$$\frac{d\sigma_{\text{Ruth}}}{d\Omega} = \left( \frac{zZ\hbar c}{4} \right)^2 \left( \frac{\alpha}{E_K} \right)^2 \frac{1}{\sin^4 \frac{\theta}{2}}, \quad (2.39)$$

allowing us to conclude that the Rutherford differential scattering cross section  $|d\sigma_{\text{Ruth}}/d\Omega|$  is:

1. Proportional to the atomic number  $z$  of the projectile and the atomic number  $Z$  of the target.
2. Proportional to the electromagnetic coupling (fine structure) constant  $\alpha^2$ . Thus, the electromagnetic force is governed by photon exchange between the  $\alpha$  particle and the nucleus.
3. Inversely proportional to the square of the initial kinetic energy  $E_K$  of the  $\alpha$  particle.
4. Inversely proportional to the fourth power of  $\sin(\theta/2)$  arising from the  $1/r^2$  variation of the Coulomb repulsive force in effect between the  $\alpha$  particle and the nucleus.

At small scattering angles  $\theta$ , where  $\sin(\frac{1}{2}\theta) \approx \frac{1}{2}\theta$ , the differential Rutherford cross section (2.38) can be simplified to read

$$\frac{d\sigma_{\text{Ruth}}}{d\Omega} = \frac{D_{\alpha-N}^2}{\theta^4}. \quad (2.40)$$

Since most of the Rutherford scattering occurs for  $\theta \ll 1$  rad and even at  $\theta = \frac{1}{2}\pi$  the small angle result is within 30 % of the general Rutherford expression, it is reasonable to use the small angle approximation of (2.40) at all angles for which the unscreened point-Coulomb field expression is valid. Departures from the point Coulomb field approximation appear for large and small angles  $\theta$ , corresponding to small and large impact parameters  $b$ , respectively, and resulting from  $\alpha$ -particle penetration of the nucleus and nuclear field screening by orbital electrons, respectively.

### 2.4.2 Differential Cross Section for Rutherford Scattering (Quantum-Mechanical Derivation)

The Rutherford differential cross section  $d\sigma_{\text{Ruth}}/d\Omega$  of (2.38) was derived classically; however, it can also be derived quantum-mechanically in a short and simple manner by using the Fermi second golden rule, discussed in Sect. 1.23.5, and the Born collision formula, discussed in Sect. 1.23.6. The Born collision formula was introduced in a general form in (1.129) and can be written for Rutherford scattering in terms of the spherically symmetric Coulomb nuclear potential  $V_N(r)$  playing the role of the potential operator  $V(r)$

$$V(r) = V_N(r) = \left( \frac{zZe^2}{4\pi\epsilon_0} \right) \frac{1}{r}. \quad (2.41)$$

For Rutherford scattering, (1.129) is expressed as follows

$$\begin{aligned} \frac{d\sigma_{\text{Ruth}}}{d\Omega} &= \left| \frac{2m_\alpha}{\hbar^2} \int_0^\infty r^2 \frac{zZe^2}{4\pi\epsilon_0} \frac{\sin(Kr)}{K^2r^2} d(Kr) \right|^2 \\ &= \left( \frac{D_{\alpha-N}}{4} \right)^2 \frac{1}{\sin^4 \frac{\theta}{2}} \left| \int_0^\infty \sin(Kr) d(Kr) \right|^2, \end{aligned} \quad (2.42)$$

after inserting the expression for nuclear Coulomb potential  $V_N(r)$  given in (2.41), expression for  $K$  given in (1.124), and the expression for  $D_{\alpha-N}$  given in (2.12).

The value of the integral in (2.42) poses a problem at its upper limit, since it oscillates about zero there. This problem can be obviated by accounting for screening effects or simply by substituting into (2.42) the nuclear Coulomb potential  $V_N(r)$  of (2.41) by a Yukawa type potential  $V_{\text{Yuk}}(r)$  where

$$V_{\text{Yuk}}(r) = V_N(r) e^{-\eta r} = \frac{zZe^2}{4\pi\epsilon_0} \frac{1}{r} e^{-\eta r}, \quad (2.43)$$

to get

$$\frac{d\sigma_{\text{Ruth}}}{d\Omega} = \left( \frac{D_{\alpha-N}}{4} \right)^2 \frac{1}{\sin^4 \frac{\theta}{2}} \left| K \int_0^\infty e^{-\eta r} \sin(Kr) dr \right|^2, \quad (2.44)$$

with  $\eta$  a positive constant which is set to zero upon solving (2.44). The integral in (2.44) in the limit  $\eta \rightarrow 0$  gives

$$\begin{aligned} \lim_{\eta \rightarrow 0} \int_0^\infty e^{-\eta r} \sin(Kr) dr &= \lim_{\eta \rightarrow 0} \left[ e^{-\eta r} \frac{-\eta \sin Kr - K \cos Kr}{\eta^2 + K^2} \right]_0^\infty \\ &= \lim_{\eta \rightarrow 0} \frac{K}{\eta^2 + K^2} = \frac{1}{K}, \end{aligned} \quad (2.45)$$

and (2.44) then gives the standard well known result for the Rutherford differential cross section derived classically in Sect. 2.4.1 and presented in (2.38) as

$$\frac{d\sigma_{\text{Ruth}}}{d\Omega} = \left( \frac{D_{\alpha\text{-N}}}{4} \right)^2 \frac{1}{\sin^4 \frac{\theta}{2}}. \quad (2.46)$$

### 2.4.3 Screening of Nuclear Potential by Orbital Electrons

At large impact parameters  $b$  (i.e., at small scattering angles  $\theta$ ) the screening effects of the atomic orbital electrons cause the potential felt by the  $\alpha$  particle to fall off more rapidly than the  $1/r$  Coulomb point-source potential. It is convenient to account for electron screening of the nuclear potential with the Thomas–Fermi statistical model of the atom in which the *Thomas–Fermi atomic potential* is given as

$$V_{\text{TF}}(r) \approx \frac{zZe^2}{4\pi\epsilon_0} \frac{1}{r} e^{-\frac{r}{a_{\text{TF}}}}. \quad (2.47)$$

In (2.47)  $a_{\text{TF}}$  is the Thomas–Fermi atomic radius expressed as

$$a_{\text{TF}} = \frac{\xi a_0}{\sqrt[3]{Z}}, \quad (2.48)$$

where

- $\xi$  is the Thomas–Fermi atomic radius constant,
- $a_0$  is the Bohr atomic radius ( $a_0 = 0.53 \text{ \AA}$ ), discussed in Sect. 3.1.1,
- $Z$  is the atomic number of the atom.

The Thomas–Fermi radius  $a_{\text{TF}}$  represents a fixed fraction of all atomic electrons or, more loosely, the radius of the atomic electron cloud that effectively screens the nucleus. The nuclear screening implies that, with a decreasing scattering angle  $\theta$ , the scattering cross-section will flatten off at small angles  $\theta$  to a finite value at  $\theta = 0$  rather than increasing as  $\theta^{-4}$  and exhibiting a singularity at  $\theta = 0$ . The constant  $\xi$  in (2.48) calculated from the Thomas–Fermi atomic model has a value of 0.885, while Jackson recommends a value of 1.4 as a better description of a general range of atomic and nuclear phenomena.

For our purposes  $\xi \approx 1$  is a good and simple approximation to yield the following expression for the Thomas–Fermi radius  $a_{\text{TF}}$

$$a_{\text{TF}} \approx \frac{a_0}{\sqrt[3]{Z}}, \quad (2.49)$$

suggesting that the effective radius of the atomic electron charge cloud decreases with an increasing atomic number  $Z$  as  $1/\sqrt[3]{Z}$ , decreasing from  $\sim a_0$  for low  $Z$  to  $\sim 0.2a_0$  for high  $Z$  elements. At first glance this result seems surprising considering that the radius of atoms increases with  $Z$ , as shown in (3.39). However, the radii of lower level atomic shells are inversely proportional to  $Z$  and this in turn results in a decreasing effective charge radius  $a_{\text{TF}}$  with increasing  $Z$ .

The Fermi second golden rule (Sect. 1.23.5) can be used in conjunction with the Born approximation (Sect. 1.23.6) to calculate  $d\sigma_{\text{Ruth}}/d\Omega$  for very small scattering angles  $\theta$  approaching 0 where (2.38) and (2.40) exhibit a singularity and predict  $d\sigma_{\text{Ruth}}/d\Omega = \infty$ , an obviously unacceptable result. Using the Thomas–Fermi potential of (2.47) for the potential  $V(r)$ , the differential cross section for Rutherford scattering is expressed as

$$\frac{d\sigma_{\text{Ruth}}}{d\Omega} = \left| \frac{2m_\alpha}{\hbar^2} \int_0^\infty r^2 V_{\text{TF}}(r) \frac{\sin(Kr)}{Kr} dr \right|^2 = \left| \frac{2m_\alpha}{\hbar^2} \frac{zZe^2}{4\pi\epsilon_0} \int_0^\infty e^{-\frac{r}{a_{\text{TF}}}} \frac{\sin(Kr)}{Kr} dr \right|^2. \quad (2.50)$$

In standard tables of integrals we find the following solution for the integral in (2.50)

$$\int_0^\infty e^{-ax} \sin(bx) dx = - \left[ \frac{e^{-ax}}{a^2 + b^2} [a \sin(bx) + b \cos(bx)] \right]_{x=0}^{x=\infty} \quad (2.51)$$

and with its help we evaluate the integral in (2.50) as

$$\int_0^\infty e^{-\frac{r}{a_{\text{TF}}}} \sin(Kr) dr = \frac{K}{\frac{1}{a_{\text{TF}}^2} + K^2} = \frac{1}{K \left[ 1 + \frac{1}{(Ka_{\text{TF}})^2} \right]}. \quad (2.52)$$

The differential cross section for the Rutherford scattering  $d\sigma_{\text{Ruth}}/d\Omega$  is now expressed as

$$\frac{d\sigma_{\text{Ruth}}}{d\Omega} = \left| \frac{2m_\alpha}{\hbar^2} \frac{zZe^2}{4\pi\epsilon_0} \frac{1}{K^2} \frac{1}{1 + \frac{1}{(Ka_{\text{TF}})^2}} \right|^2. \quad (2.53)$$

The term  $[1 + (Ka_{\text{TF}})^{-2}]^{-2}$  may be regarded as a correction factor to the standard differential scattering cross section (2.46) for  $\theta \rightarrow 0$  where the

Thomas–Fermi screening of the simple point-source Coulomb nuclear potential becomes important. The product  $Ka_{\text{TF}}$  using the expression for  $K$  of (1.124) is now given as

$$Ka_{\text{TF}} = \frac{2pa_{\text{TF}}}{\hbar} \sin \frac{\theta}{2} \quad (2.54)$$

and for a typical Rutherford scattering experiment using naturally emitted  $\alpha$  particles on a gold foil amounts to  $\sim 10^5 \sin(\theta/2)$ . Thus, unless the scattering angle is very small, the correction factor  $[1 + (Ka_{\text{TF}})^{-2}]^{-2}$  is equal to 1 and (2.53) transforms into the simple Rutherford relationship given in (2.38). Equation (2.53) is then simplified to read

$$\begin{aligned} \frac{d\sigma_{\text{Ruth}}}{d\Omega} &= \left| \frac{2m_\alpha zZe^2}{\hbar^2} \frac{1}{4\pi\epsilon_0} \frac{1}{K^2} \right|^2 = \left| \frac{2m_\alpha zZe^2}{\hbar^2} \frac{1}{4\pi\epsilon_0} \frac{\hbar^2}{4p^2 \sin^2(\theta/2)} \right|^2 \\ &= \left( \frac{D_{\alpha\text{-N}}}{4} \right)^2 \frac{1}{\sin^4 \frac{\theta}{2}} \end{aligned} \quad (2.55)$$

and shows that the Rutherford scattering formula for a point-charge Coulomb field approximation can also be derived through quantum mechanical reasoning using the Fermi second golden rule and the Born approximation but neglecting any magnetic interaction involving spin effects.

#### 2.4.4 Minimum Scattering Angle

We now return to (2.53) to show that for very small scattering angles  $\theta$  it provides a finite result for  $d\sigma_{\text{Ruth}}/d\Omega$  in contrast to the singularity exhibited by (2.55). The general differential cross section  $d\sigma_{\text{Ruth}}/d\Omega$  including the small- $\theta$  correction factor  $[1 + (Ka_{\text{TF}})^{-2}]^{-2}$  is

$$\frac{d\sigma_{\text{Ruth}}}{d\Omega} = \left( \frac{D_{\alpha\text{-N}}}{4} \right)^2 \frac{1}{\sin^4 \frac{\theta}{2}} \frac{1}{\left[ 1 + \frac{1}{(Ka_{\text{TF}})^2} \right]^2} \approx \frac{D_{\alpha\text{-N}}^2}{\theta^4} \frac{1}{\left[ 1 + \left( \frac{\hbar}{pa_{\text{TF}}\theta} \right)^2 \right]^2}, \quad (2.56)$$

after introducing the expression for  $K$  given in (2.54) and using the approximation  $\sin \theta \approx \theta$  for small scattering angles  $\theta$ .

Next we introduce the concept of  $\theta_{\text{min}}$ , the minimum cutoff scattering angle for a given scattering experiment. Using the expressions for  $p$  and  $a_{\text{TF}}$  given by (1.64) and (2.49), respectively, we define  $\theta_{\text{min}}$  as

$$\theta_{\text{min}} = \frac{\hbar}{pa_{\text{TF}}} = \frac{\hbar\sqrt[3]{Z}}{pa_0} = \frac{\hbar c\sqrt[3]{Z}}{a_0\sqrt{E_{\text{K}}(E_{\text{K}} + 2E_0)}}, \quad (2.57)$$

where

$E_K$  is the kinetic energy of the  $\alpha$  particle,  
 $E_0$  is the rest energy of the  $\alpha$  particle (3727.4 MeV).

Quantum-mechanically, based on Heisenberg uncertainty principle of (1.130), we define the minimum cutoff angle  $\theta_{\min}$  (also referred to as the Born screening angle) as follows: When the classical trajectory of the incident particle is localized within  $\Delta z \approx a_{\text{TF}}$ , the corresponding uncertainty on the transverse momentum of the particle is  $\Delta p \geq \hbar/a_{\text{TF}}$ , resulting in

$$\theta_{\min} = \frac{\Delta p}{p} \approx \frac{\hbar}{pa_{\text{TF}}} = \frac{\lambda}{a_{\text{TF}}}. \quad (2.58)$$

For small scattering angles  $\theta$  including  $\theta = 0$  the differential scattering cross section  $d\sigma_{\text{Ruth}}/d\Omega$  given in (2.56) simplifies to

$$\frac{d\sigma_{\text{Ruth}}}{d\Omega} = \frac{D_{\alpha\text{-N}}^2}{[\theta^2 + \theta_{\min}^2]^2}, \quad (2.59)$$

and converges to the following finite value for  $\theta = 0$

$$\frac{d\sigma_{\text{Ruth}}}{d\Omega} = \frac{D_{\alpha\text{-N}}^2}{\theta_{\min}^4}. \quad (2.60)$$

### 2.4.5 Effect of the Finite Size of the Nucleus

At relatively large scattering angles  $\theta$  the differential cross section  $d\sigma_{\text{Ruth}}/d\Omega$  is smaller than that predicted by (2.38) because of the finite size of the nucleus. Approximating the charge distribution of the atomic nucleus by a volume distribution inside a sphere of radius  $R$  results in the following electrostatic potentials  $V(r)$  for regions inside and outside the nucleus

$$V(r) = \frac{zZe^2}{4\pi\epsilon_0 R} \left( \frac{3}{2} - \frac{1}{2} \frac{r^2}{R^2} \right) \quad \text{for } r < R \text{ (inside the nucleus)}, \quad (2.61)$$

$$V(r) = \frac{3}{8} \frac{zZe^2}{\pi\epsilon_0 R} \quad \text{for } r = 0 \text{ (at the center of the nucleus)}, \quad (2.62)$$

$$V(r) = \frac{zZe^2}{4\pi\epsilon_0 R} \quad \text{for } r = R \text{ (at the edge of the nucleus)}, \quad (2.63)$$

$$V(r) = \frac{zZe^2}{4\pi\epsilon_0 r} \quad \text{for } r > R \text{ (outside the nucleus)}. \quad (2.64)$$

For use in the Fermi golden rule in conjunction with the Born approximation the four functions above can be approximated with the following single function  $V_{\text{FNS}}(r)$  approximating the effects of the finite nuclear size (FNS) and covering the whole region of  $r$  from 0 to  $\infty$

$$V_{\text{FNS}}(r) = \frac{zZe^2}{4\pi\epsilon_0} \frac{1}{r} \left(1 - e^{-2r/R}\right), \tag{2.65}$$

where  $R$  is the nominal radius of the nucleus calculated from  $R = R_o \sqrt[3]{A}$ , given in (1.26).

In Fig. 2.5 the potential energy  $V_{\text{FNS}}$  is plotted against  $r$ , the distance from the center of the nucleus, for the gold nucleus. It converges to  $(2zZe^2) / (4\pi\epsilon_0 R)$  at  $r = 0$  and provides a reasonable and continuous approximation both inside the finite nucleus where  $r \leq R$  and outside the nucleus for  $r > R$  where the point source Coulomb approximation holds.

For comparison, also shown in Fig. 2.5 are the Coulomb point source potential (dashed curve) and the finite source potential assuming a uniform charge distribution inside the nuclear sphere with radius  $R$  (light solid curve). At  $r = 0$  the Coulomb source potential exhibits a singularity and the finite source with uniform charge density converges to  $(3zZe^2) / (8\pi\epsilon_0 R)$ , as shown in (2.62). For the gold nucleus  $V_{\text{FNS}}$  at  $r = 0$  converges to 64.9 MeV and the

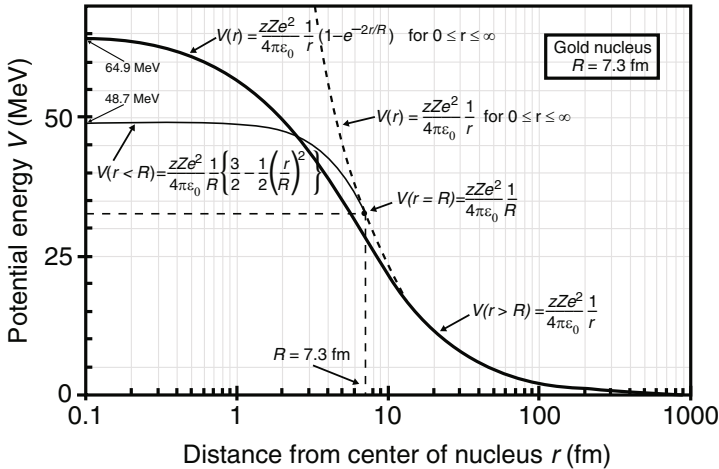


**Fig. 2.5.** Potential energy  $V(r)$  against distance  $r$  from the center of gold nucleus with radius  $R = 7.3$  fm. Three different potential energies are plotted: (1) Point source nuclear potential  $V_{\text{N}}(r)$  of (2.41) shown with dashed curve exhibiting singularity at  $r = 0$ ; (2) Potential for uniform charge distribution inside nuclear sphere of (2.61) shown with light solid curve and converging to  $(3zZe^2)/(8\pi\epsilon_o R) = 48.7$  MeV at  $r = 0$ ; and (3) Exponential function potential  $V_{\text{FNS}}(r)$  of (2.65) approximating potential inside and outside the finite size nucleus, shown with heavy solid curve, and converging to  $(zZe^2)/(2\pi\epsilon_o R) = 64.9$  MeV at  $r = 0$

field assuming a uniform charge distribution inside the nucleus converges to 48.7 MeV, as shown in Fig. 2.5.

Inserting (2.65) into the Born approximation of (1.129) results in the following integral for  $d\sigma_{\text{Ruth}}/d\Omega$

$$\begin{aligned} \frac{d\sigma_{\text{Ruth}}}{d\Omega} &= \left| \frac{2m_\alpha}{\hbar^2} \int_0^\infty r^2 V_{\text{FNS}}(r) \frac{\sin(Kr)}{Kr} dr \right|^2 \\ &= \left| \frac{2m_\alpha}{\hbar^2} \frac{zZe^2}{4\pi\epsilon_0 K} \int_0^\infty \left(1 - e^{-\frac{2r}{R}}\right) \sin(Kr) dr \right|^2 \\ &= \left| \frac{2m_\alpha}{\hbar^2} \frac{zZe^2}{4\pi\epsilon_0 K} \left\{ \int_0^\infty \sin(Kr) dr - \int_0^\infty e^{-\frac{2r}{R}} \sin(Kr) dr \right\} \right|^2. \end{aligned} \quad (2.66)$$

The integrals in the curly bracket of (2.66) are calculated using (2.51) to get

$$\begin{aligned} &\left\{ \int_0^\infty \sin(Kr) dr - \int_0^\infty e^{-\frac{2r}{R}} \sin(Kr) dr \right\} \\ &= \left[ -\frac{\cos(Kr)}{K} + \frac{e^{-\frac{2r}{R}} [2R^{-1} \sin(Kr) + K \cos(Kr)]}{\frac{4}{R^2} + K^2} \right]_{r=0}^{r=\infty} \\ &= \frac{1}{K} - \frac{K}{\frac{4}{R^2} + K^2} = \frac{1}{K \left(1 + \frac{K^2 R^2}{4}\right)}. \end{aligned} \quad (2.67)$$

### 2.4.6 Maximum Scattering Angle

The differential cross section  $d\sigma_{\text{Ruth}}/d\Omega$  after inserting (2.67) into (2.66) is given as

$$\begin{aligned} \frac{d\sigma_{\text{Ruth}}}{d\Omega} &= \left| \frac{2m_\alpha}{\hbar^2} \frac{zZe^2}{4\pi\epsilon_0} \frac{1}{K^2} \frac{1}{\left(1 + \frac{K^2 R^2}{4}\right)} \right|^2 \\ &= \left( \frac{D_{\alpha\text{-N}}}{4} \right)^2 \frac{1}{\sin^4 \frac{\theta}{2}} \frac{1}{\left[ 1 + \left( \frac{pR \sin(\frac{1}{2}\theta)}{\hbar} \right)^2 \right]^2} \\ &= \left( \frac{D_{\alpha\text{-N}}}{4} \right)^2 \frac{1}{\sin^4 \frac{\theta}{2}} \frac{1}{\left[ 1 + \left( \frac{\sin(\frac{1}{2}\theta)}{\theta_{\text{max}}} \right)^2 \right]^2}, \end{aligned} \quad (2.68)$$

after first inserting the expression for  $K = 2(p/\hbar) \sin(\theta/2)$  of (1.124) and then defining the maximum (cutoff) scattering angle  $\theta_{\max}$ , beyond which the scattering cross section falls significantly below the  $\sin^{-4}(\frac{1}{2}\theta)$  expression, as

$$\theta_{\max} = \frac{\hbar}{pR} = \frac{\hbar c}{R_0 \sqrt[3]{A} \sqrt{E_K (E_K + 2E_0)}}, \quad (2.69)$$

where again

$E_K$  is the kinetic energy of the  $\alpha$  particle,  
 $E_0$  is the rest energy of the  $\alpha$  particle (3727.4 MeV).

The maximum cutoff scattering angle  $\theta_{\max}$  can be defined quantum-mechanically based on the Heisenberg uncertainty principle of (1.130) as follows: When the classical trajectory of the incident particle is localized within  $\Delta z \approx R$ , the corresponding uncertainty on the transverse momentum of the particle is  $\Delta p \geq \hbar/R$ , leading to

$$\theta_{\max} = \frac{\Delta p}{p} \approx \frac{\hbar}{pR} = \frac{\lambda}{R} = \frac{\lambda}{2\pi R}, \quad (2.70)$$

where  $\lambda$  is the de Broglie wavelength of the incident  $\alpha$  particle and we assume that  $\theta_{\max} \ll 1$ .

### 2.4.7 General Relationships for Differential Cross Section in Rutherford Scattering

In each Rutherford collision the angular deflections obey the Rutherford expression with cutoff at  $\theta_{\min}$  and  $\theta_{\max}$  given by (2.57) and (2.69), respectively. The typical value for  $\hbar/p$  in the two expressions can be estimated for  $\alpha$  particles with a typical kinetic energy of 5.5 MeV as follows

$$\frac{\hbar}{p} = \frac{\hbar c}{\sqrt{E_K (E_K + 2E_0)}} \approx \frac{197.3 \text{ MeV} \cdot \text{fm}}{\sqrt{5.5 (5.5 + 2 \times 3727.4) \text{ MeV}}} \approx 1 \text{ fm}, \quad (2.71)$$

where we use the expression for  $p$  given in (1.64). Inserting the value for  $\hbar/p \approx 1 \text{ fm}$  into (2.58) and (2.69), respectively, for a typical  $\alpha$  particle kinetic energy of 5.5 MeV, combined with appropriate values for  $a_{\text{TF}} = 0.123 \times 10^5 \text{ fm}$  and  $R = 7.3 \text{ fm}$ , results in the following angles  $\theta_{\min}$  and  $\theta_{\max}$  for the gold atom

$$\theta_{\min} = \frac{\hbar}{pa_{\text{TF}}} = \frac{\hbar c \sqrt[3]{Z}}{pc a_0} \approx (1 \text{ fm}) \frac{\sqrt[3]{79}}{0.5292 \times 10^5 \text{ fm}} \approx 8.1 \times 10^{-5} \text{ rad} \quad (2.72)$$

and

$$\theta_{\max} = \frac{\hbar}{pR} = \frac{\hbar c}{pc R_0 \sqrt[3]{A}} \approx (1 \text{ fm}) \frac{1}{(1.25 \text{ fm}) \sqrt[3]{197}} \approx 0.14 \text{ rad}. \quad (2.73)$$

We now see that the Rutherford scattering of  $\alpha$  particles on nuclei is governed by the following stipulation:  $\theta_{\min} \ll \theta_{\max} \ll 1$ , justifying our assumptions in (2.58) and (2.70) that both cutoff angles are much smaller than 1. We also note that the ratio  $\theta_{\max}/\theta_{\min}$  is independent of  $\alpha$  particle kinetic energy  $E_K$  but depends on the atomic number  $Z$  and mass number  $A$  of the scatterer and is given as

$$\frac{\theta_{\max}}{\theta_{\min}} = \frac{a_{\text{TF}}}{R} \approx \frac{a_0}{R_0 \sqrt[3]{ZA}} = \frac{0.5292 \times 10^5 \text{ fm}}{1.25 \text{ fm}} \frac{1}{\sqrt[3]{ZA}} \approx \frac{0.423 \times 10^5}{\sqrt[3]{ZA}}. \quad (2.74)$$

From (2.74) we estimate that the ratio  $\theta_{\max}/\theta_{\min}$  ranges from  $\sim 5 \times 10^4$  for low atomic number  $Z$  scatterers to  $\sim 1.5 \times 10^3$  for high atomic number  $Z$  scatterers, since  $\sqrt[3]{ZA}$  ranges from 1 at low  $Z$  to about 30 at high  $Z$ . We may thus conclude that  $\theta_{\max}/\theta_{\min} \gg 1$  for all elements. For gold, the material used in Geiger–Marsden experiment,  $\sqrt[3]{ZA}$  amounts to  $\sim 1.76 \times 10^3$ .

The differential cross section  $d\sigma_{\text{Ruth}}/d\Omega$  for Rutherford scattering of 5.5 MeV  $\alpha$  particles on gold nuclei is plotted in Fig. 2.6 in the form  $(D_{\alpha-N}^{-2}) d\sigma_{\text{Ruth}}/d\Omega$  against the scattering angle  $\theta$  in the range from  $10^{-5}$  rad to  $\pi$ . As calculated in (2.72) and (2.73),  $\theta_{\min} = 8.1 \times 10^{-5}$  rad and  $\theta_{\max} = 0.14$  rad, respectively. Three distinct regions can be identified on the graph: small  $\theta$ ; intermediate  $\theta$ ; and large  $\theta$ .

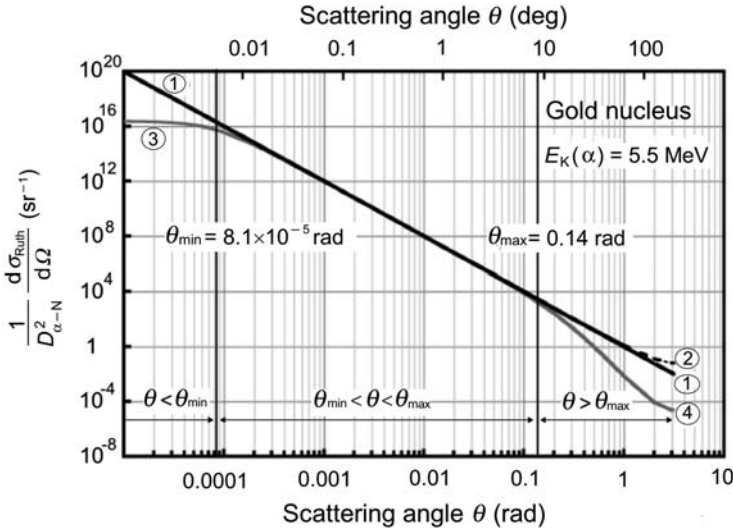


**Fig. 2.6.** Differential Rutherford scattering cross section  $[(1/D_{\alpha-N}^2) \times (d\sigma_{\text{Ruth}}/d\Omega)]$  plotted against the scattering angle  $\theta$  for 5.5 MeV  $\alpha$  particles interacting with gold. The minimum and maximum scattering angles  $\theta_{\min} = 8.1 \times 10^{-5}$  rad and  $\theta_{\max} = 0.14$  rad, respectively, are identified. For  $\theta \rightarrow 0$  the value of the ordinate approaches  $(1/\theta_{\min}^4) \approx 2.32 \times 10^{16} \text{ (rad)}^{-4}$

1. In the intermediate region  $\theta_{\min} \ll \theta \ll \theta_{\max}$  where  $\theta_{\min} \ll \theta_{\max} \ll 1$ , the simple Rutherford differential scattering expressions given by (2.38) and (2.40) apply, resulting in a straight line [curves (1) and (2)] on the log-log plot

$$\frac{1}{D_{\alpha-N}^2} \frac{d\sigma_{\text{Ruth}}}{d\Omega} = \frac{1}{16} \frac{1}{\sin^4(\theta/2)} \approx \frac{1}{\theta^4}. \quad (2.75)$$

2. In the small angle  $\theta$  region ( $\theta < \theta_{\min}$ ), as a result of nuclear screening and after applying the Thomas-Fermi atomic model, the differential cross section is given by

$$\frac{1}{D_{\alpha-N}^2} \frac{d\sigma_{\text{Ruth}}}{d\Omega} = \frac{1}{(\theta^2 + \theta_{\min}^2)^2}, \quad (2.76)$$

resulting in curve (3) in Fig. 2.6 and converging to a finite value of  $\theta_{\min}^{-4} = 2.32 \times 10^{16} \text{ rad}^{-4}$  for  $\theta = 0$ .

3. In the large angle  $\theta$  region where  $\theta > \theta_{\max}$ , (2.40) represented by curve (1) is still linear, while (2.38) results in curve (2). A correction for finite nuclear size and nuclear penetration of the scattered particle lowers the value of the differential cross section from the value predicted by the simple Rutherford equation and results from (2.68) in

$$\frac{1}{D_{\alpha-N}^2} \frac{d\sigma_{\text{Ruth}}}{d\Omega} = \frac{1}{16} \frac{1}{\sin^4(\theta/2)} \frac{1}{\left(1 + \frac{\sin^2(\theta/2)}{\theta_{\max}^2}\right)^2}, \quad (2.77)$$

shown as curve (4) in Fig. 2.6.

### 2.4.8 Total Rutherford Scattering Cross Section

The total cross section for Rutherford scattering can be approximated by using the small angle approximation and integrating (2.59) over the complete solid angle to obtain

$$\begin{aligned} \sigma_{\text{Ruth}} &= \int \frac{d\sigma_{\text{Ruth}}}{d\Omega} d\Omega = 2\pi \int_0^{\theta_{\max}} \frac{d\sigma_{\text{Ruth}}}{d\Omega} \sin \theta d\theta \approx 2\pi D_{\alpha-N}^2 \int_0^{\theta_{\max}} \frac{\theta d\theta}{(\theta^2 + \theta_{\min}^2)^2} \\ &= \pi D_{\alpha-N}^2 \int_0^{\theta_{\max}} \frac{d(\theta^2 + \theta_{\min}^2)}{(\theta^2 + \theta_{\min}^2)^2} = \pi D_{\alpha-N}^2 \left\{ \frac{1}{\theta_{\min}^2} - \frac{1}{\theta_{\max}^2 + \theta_{\min}^2} \right\} \\ &= \pi D_{\alpha-N}^2 \frac{1}{\theta_{\min}^2} \left\{ 1 - \frac{1}{1 + \left(\frac{\theta_{\max}}{\theta_{\min}}\right)^2} \right\}. \end{aligned} \quad (2.78)$$

In each Rutherford collision the angular deflections obey the Rutherford expression with cutoffs at  $\theta_{\min}$  and  $\theta_{\max}$  given by (2.72) and (2.73), respectively. The typical value for  $\hbar/p$  in the expressions for  $\theta_{\min}$  and  $\theta_{\max}$  was estimated in (2.71) for  $\alpha$  particles with a typical kinetic energy of 5.5 MeV as 1 fm while  $\theta_{\min}$  and  $\theta_{\max}$  for gold atom were estimated in (2.72) and (2.73) as  $8.1 \times 10^{-5}$  rad and 0.14 rad, respectively. The cutoff angles  $\theta_{\min}$  and  $\theta_{\max}$  thus satisfy the Rutherford condition stipulating that  $\theta_{\min} \ll \theta_{\max} \ll 1$  and, since also  $\theta_{\max}/\theta_{\min} \gg 1$ , the total cross section for Rutherford scattering given in (2.78) can be simplified, after inserting (2.12) and (2.57), to read

$$\sigma_{\text{Ruth}} \approx \frac{\pi D_{\alpha\text{-N}}^2}{\theta_{\min}^2} = \pi a_{\text{TF}}^2 \left( \frac{D_{\alpha\text{-N}}}{(\hbar/p)} \right)^2 = \pi a_{\text{TF}}^2 \left\{ \frac{2zZe^2}{4\pi\epsilon_0\hbar v_i} \right\}^2. \quad (2.79)$$

The parameters of (2.79) are as follows:

- $a_{\text{TF}}$  is the Thomas–Fermi atomic radius
- $Z$  is the atomic number of the absorber foil,
- $z$  is the atomic number of the  $\alpha$  particle,
- $v_i$  is the initial velocity of the  $\alpha$  particle, equal to the final velocity of the  $\alpha$  particle
- $D_{\alpha\text{-N}}$  is the distance of closest approach between the  $\alpha$  particle and nucleus in a direct-hit head-on collision ( $b = 0$ ).

For the Geiger–Marsden experiment with 5.5 MeV  $\alpha$  particles scattered on a  $1 \mu\text{m}$  thick gold foil we calculate the following total scattering cross section

$$\sigma_{\text{Ruth}} = \frac{\pi D_{\alpha\text{-N}}^2}{\theta_{\min}^2} = \frac{\pi (41 \times 10^{-13} \text{ cm})^2}{(8.1 \times 10^{-5})^2} = 8.05 \times 10^9 \text{ b}. \quad (2.80)$$

### 2.4.9 Mean Square Scattering Angle for Single Rutherford Scattering

Rutherford scattering is confined to very small angles and for energetic  $\alpha$  particles  $\theta_{\max} \ll 1$  rad. An  $\alpha$  particle traversing a gold foil will undergo a large number of small angle  $\theta$  scatterings and emerge from the foil with a small cumulative angle  $\Theta$  that represents a statistical superposition of a large number of small angle deflections.

Large angle scattering events, on the other hand, are rare and a given  $\alpha$  particle will undergo at most only one such rare scattering event while traversing the gold foil. As discussed in Sect. 2.2, Geiger and Marsden found that only about 1 in  $10^4$   $\alpha$  particles traverses the  $1 \mu\text{m}$  thick gold foil with a scattering angle  $\Theta$  exceeding  $90^\circ$ . The range of Rutherford angular scattering is thus divided into two distinct regions:

1. Single scattering events with large angle  $\theta$ .
2. Multiple scattering events resulting in a small cumulative angle  $\Theta$ .

In the multiple-scatter region, the mean square angle for single scattering  $\overline{\theta^2}$  is

$$\overline{\theta^2} = \frac{\int \theta^2 \frac{d\sigma_{\text{Ruth}}}{d\Omega} d\Omega}{\int \frac{d\sigma_{\text{Ruth}}}{d\Omega} d\Omega} = \frac{\int \theta^2 \frac{d\sigma_{\text{Ruth}}}{d\Omega} d\Omega}{\sigma_{\text{Ruth}}}. \quad (2.81)$$

The denominator in (2.81) is the total Rutherford scattering cross section  $\sigma_{\text{Ruth}}$ , given in (2.79). It is proportional to the square of the distance of closest approach  $(D_{\alpha-N})^2$  and inversely proportional to  $\theta_{\text{min}}^2$ . The integral in the numerator of (2.81) is in the small angle approximation ( $\sin \theta \approx \theta$ ) calculated as follows

$$\begin{aligned} \int \theta^2 \frac{d\sigma_{\text{Ruth}}}{d\Omega} d\Omega &= 2\pi D_{\alpha-N}^2 \int_0^{\theta_{\text{max}}} \frac{\theta^2 \sin \theta d\theta}{(\theta^2 + \theta_{\text{min}}^2)^2} \approx 2\pi D_{\alpha-N}^2 \int_0^{\theta_{\text{max}}} \frac{\theta^3 d\theta}{(\theta^2 + \theta_{\text{min}}^2)^2} \\ &= \pi D_{\alpha-N}^2 \int_0^{\theta_{\text{max}}} \frac{(\theta^2 + \theta_{\text{min}}^2) d(\theta^2 + \theta_{\text{min}}^2)}{(\theta^2 + \theta_{\text{min}}^2)^2} - \pi D_{\alpha-N}^2 \int_0^{\theta_{\text{max}}} \frac{\theta_{\text{min}}^2 d(\theta^2 + \theta_{\text{min}}^2)}{(\theta^2 + \theta_{\text{min}}^2)^2} \\ &= \pi D_{\alpha-N}^2 \left\{ \ln(\theta^2 + \theta_{\text{min}}^2) + \frac{\theta_{\text{min}}^2}{\theta^2 + \theta_{\text{min}}^2} \right\}_0^{\theta_{\text{max}}} \\ &= \pi D_{\alpha-N}^2 \left\{ \ln \left( 1 + \frac{\theta_{\text{max}}^2}{\theta_{\text{min}}^2} \right) + \frac{\theta_{\text{min}}^2}{\theta_{\text{max}}^2 + \theta_{\text{min}}^2} - 1 \right\}. \end{aligned} \quad (2.82)$$

The mean square angle  $\overline{\theta^2}$  of (2.81) for a single scattering event, after incorporating the Rutherford total scattering cross section given in (2.79), is then given by the following relationship

$$\overline{\theta^2} = \theta_{\text{min}}^2 \ln \left( 1 + \frac{\theta_{\text{max}}^2}{\theta_{\text{min}}^2} \right) - \frac{\theta_{\text{min}}^2 \theta_{\text{max}}^2}{\theta_{\text{min}}^2 + \theta_{\text{max}}^2} = \theta_{\text{min}}^2 \ln \left( 1 + \frac{\theta_{\text{max}}^2}{\theta_{\text{min}}^2} \right) - \left( \frac{1}{\theta_{\text{min}}^2} + \frac{1}{\theta_{\text{max}}^2} \right)^{-1}. \quad (2.83)$$

The expression in (2.83) can be simplified using Rutherford scattering condition stipulating that  $\theta_{\text{min}} \ll \theta_{\text{max}} \ll 1$  to obtain

$$\overline{\theta^2} \approx 2 \theta_{\text{min}}^2 \ln \frac{\theta_{\text{max}}}{\theta_{\text{min}}}. \quad (2.84)$$

For the Geiger–Marsden experiment with 5.5 MeV  $\alpha$  particles scattered on a gold foil we calculate the following mean square angle for single Rutherford scattering

$$\overline{\theta^2} \approx 2\theta_{\text{min}}^2 \ln \frac{\theta_{\text{max}}}{\theta_{\text{min}}} = 2 \times (8.1 \times 10^{-5} \text{ rad})^2 \ln \frac{0.14}{8.1 \times 10^{-5}} = 9.8 \times 10^{-8} (\text{rad})^2, \quad (2.85)$$

resulting in the following root mean square scattering angle

$$\sqrt{\overline{\theta^2}} = 3.13 \times 10^{-4} \text{ rad}. \quad (2.86)$$

### 2.4.10 Mean Square Scattering Angle for Multiple Rutherford Scattering

Since the successive scattering collisions are independent events, the *central-limit theorem* of statistics (see Sect. 2.7.1) shows that for a large number  $n > 20$  of such collisions, the distribution in angle will be Gaussian around the forward direction [see (2.2)] with a cumulative mean square scattering angle  $\overline{\Theta^2}$  related to the mean square scattering angle  $\overline{\theta^2}$  for a single scattering event given in (2.83). The cumulative mean square angle  $\overline{\Theta^2}$  and the mean square angle  $\overline{\theta^2}$  for a single scattering event are related as follows

$$\overline{\Theta^2} = n\overline{\theta^2} \tag{2.87}$$

where  $n$ , the number of scattering events, is

$$n = \frac{N_a}{V} \sigma_{\text{Ruth}} t = \rho \frac{N_A}{A} \sigma_{\text{Ruth}} t = \pi \rho \frac{N_A}{A} \frac{D_{\alpha-N}^2}{\theta_{\min}^2} t. \tag{2.88}$$

In (2.88) the parameters are as follows:

- $\sigma_{\text{Ruth}}$  is the total Rutherford cross section given by (2.78),
- $N_a/V$  is the number of atoms per volume equal to  $\rho N_A/A$ ,
- $\rho$  is the density of the foil material,
- $t$  is the thickness of the foil,
- $A$  is the atomic mass number,
- $N_A$  is the Avogadro number ( $N_A = 6.023 \times 10^{23} \text{ mol}^{-1}$ ),
- $D_{\alpha-N}$  is the distance of closest approach between the  $\alpha$  particle and the nucleus in a direct hit interaction where  $b = 0$  [see (2.12)],
- $\theta_{\min}$  is the cutoff angle defined in (2.57).

The mean square angle  $\overline{\Theta^2}$  of the Gaussian distribution after combining (2.85), (2.87) and (2.88) is then given by

$$\overline{\Theta^2} = 2\pi \rho \frac{N_A}{A} t D_{\alpha-N}^2 \ln \frac{\theta_{\max}}{\theta_{\min}}, \tag{2.89}$$

indicating that the mean square angle  $\overline{\Theta^2}$  for multiple Rutherford scattering increases linearly with the foil thickness  $t$ . Inserting the expressions for  $\theta_{\min}$  and  $\theta_{\max}$  of (2.57) and (2.69), respectively, into (2.89), we now get the following expression for the mean square angle  $\overline{\Theta^2}$  in Rutherford scattering

$$\overline{\Theta^2} = 2\pi \rho \frac{N_A}{A} t D_{\alpha-N}^2 \ln \frac{1.4a_0}{R_0 \sqrt[3]{AZ}} = 2\pi \rho \frac{N_A}{A} t \left\{ \frac{zZe^2}{4\pi\epsilon_0 E_K} \right\}^2 \ln \frac{1.4a_0}{R_0 \sqrt[3]{AZ}}, \tag{2.90}$$

where  $a_0 = 0.5292 \text{ \AA}$  and  $R_0 = 1.25 \text{ fm}$  are the Bohr radius constant of (3.4) and the nuclear radius constant of (1.26), respectively.

For the Geiger–Marsden experiment with 5.5 MeV  $\alpha$  particles scattered on a gold foil we calculate the following mean square angle for multiple Rutherford scattering

$$\begin{aligned}\overline{\Theta^2} &= 2\pi\rho\frac{N_A}{A}t D_{\alpha-N}^2 \ln\frac{\theta_{\max}}{\theta_{\min}} \\ &= 2\pi \times 19.3 \text{ (g/cm}^3\text{)} \frac{6.022 \times 10^{23} \text{ (mol)}^{-1}}{197 \text{ (g/mol)}} 10^{-4} \text{ cm (} 41 \times 10^{-13} \text{ cm)}^2 \\ &\quad \times \ln\frac{0.14}{8.1 \times 10^{-5}} = 46.4 \times 10^{-4} \text{ (rad)}^2,\end{aligned}\tag{2.91}$$

resulting in the following root mean square scattering angle for multiple scattering

$$\sqrt{\overline{\Theta^2}} = 0.068 \text{ rad} = 3.9^\circ.\tag{2.92}$$

#### 2.4.11 Importance of the Rutherford Scattering Experiment

Tables 2.1–2.3 summarize the parameters of the Geiger–Marsden  $\alpha$ -particle scattering experiment, listing the important parameters of the  $\alpha$  particles; the gold atom; and Rutherford scattering, respectively, based on expressions derived in this section. All data are calculated for Rutherford scattering of 5.5 MeV  $\alpha$  particles on gold nuclei.

The  $\alpha$ -particle scattering experiment on a thin gold foil conducted by Hans Geiger and Ernest Marsden under the guidance of Ernest Rutherford seems rather mundane, yet it is one of the most important experiments in the history of physics. Nature provided Geiger and Marsden with ideal conditions to probe the nucleus with radon-222  $\alpha$  particles with kinetic energy of 5.5 MeV.

**Table 2.1.** Properties of  $\alpha$  particles used in the Geiger–Marsden experiment

Properties of $\alpha$ particles	
Atomic number	$z = 2$
Rest energy	$E_0 = m_\alpha c^2 = 3727.4 \text{ MeV}$
Kinetic energy	$E_K = E - E_0 = 5.5 \text{ MeV}$
Normalized velocity	$\frac{v_\alpha}{c} = \sqrt{1 - \frac{1}{\left(1 + \frac{E_K}{m_\alpha c^2}\right)^2}} = 0.054$
Momentum	$p = \frac{1}{c}\sqrt{E^2 - E_0^2} = \frac{1}{c}\sqrt{E_K^2 + 2E_K E_0} = 202.6 \text{ MeV}/c$ (1.64)
Reduced Planck constant divided by momentum	$\frac{\hbar}{p} = \frac{\hbar c}{pc} = \frac{197.3 \text{ MeV} \cdot \text{fm}}{202.6 \text{ MeV}} = 0.974 \text{ fm} \approx 1 \text{ fm}$

**Table 2.2.** Properties of gold atom of importance in Rutherford scattering

Properties of gold atom $^{197}_{79}\text{Au}$	
Atomic number	$Z = 79$
Atomic mass number	$A = 197$
Density	$\rho = 19.3 \text{ g/cm}^3$
Thomas–Fermi radius	$a_{\text{TF}} = \frac{a_0}{\sqrt[3]{Z}} = \frac{0.5292 \text{ \AA}}{\sqrt[3]{79}} = 0.123 \text{ \AA}$ (2.49)
Nuclear radius	$R = R_0 \sqrt[3]{A} = (1.25 \text{ fm}) \sqrt[3]{197} = 7.3 \text{ fm}$ (2.13)
Thickness of gold foil	$t = 10^{-4} \text{ cm} = 1 \text{ }\mu\text{m}$

**Table 2.3.** Parameters of Geiger–Marsden experiment.  $\alpha$  particles with kinetic energy of 5.5 MeV undergo Rutherford scattering on a 1  $\mu\text{m}$  thick gold foil

Parameters of Rutherford scattering	
Distance of closest approach	$D_{\alpha-N} = \frac{zZe^2}{4\pi\epsilon_0} \frac{1}{E_K} = 41 \text{ fm}$ (2.12)
Minimum scattering angle	$\theta_{\min} = \frac{\hbar}{p} \frac{1}{a_{\text{TF}}} = \frac{1 \text{ fm}}{0.123 \times 10^5 \text{ fm}}$ $= 8.1 \times 10^{-5} \text{ rad}$ (2.72)
Maximum scattering angle	$\theta_{\max} = \frac{\hbar}{p} \frac{1}{R} = \frac{1 \text{ fm}}{7.3 \text{ fm}} \approx 0.14 \text{ rad}$ (2.73)
Ratio $\frac{\theta_{\max}}{\theta_{\min}}$	$\frac{\theta_{\max}}{\theta_{\min}} = \frac{0.14}{8.1 \times 10^{-5}} = 1.766 \times 10^3$ (2.74)
Differential Rutherford cross section at $\theta = 0$	$\left. \frac{d\sigma_{\text{Ruth}}}{d\Omega} \right _{\theta=0} = \frac{D_{\alpha-N}^2}{\theta_{\min}^4} = 3.9 \times 10^{17} \text{ b/sr}$ (2.76)
Rutherford cross section	$\sigma_{\text{Ruth}} = \pi \frac{D_{\alpha-N}^2}{\theta_{\min}^2} = 8.05 \times 10^9 \text{ b}$ (2.79)
Mean square scattering angle for single scattering	$\overline{\theta^2} \approx 2\theta_{\min}^2 \ln \frac{\theta_{\max}}{\theta_{\min}} = 9.8 \times 10^{-8} \text{ (rad)}^2$ (2.80)
Root mean square angle for single scattering	$\sqrt{\overline{\theta^2}} = 3.13 \times 10^{-4} \text{ rad}$ (2.86)
Mean square scattering angle for multiple scattering	$\overline{\theta^2} = 2\pi\rho \frac{N_A}{A} t D_{\alpha-N}^2 \ln \frac{\theta_{\max}}{\theta_{\min}} = n\overline{\theta^2}$ $= 46.4 \times 10^{-4} \text{ (rad)}^2$ (2.89)
Root mean square angle for multiple scattering	$\sqrt{\overline{\theta^2}} = 0.068 \text{ rad} = 3.9^\circ$ (2.92)
Number of scattering events	$n = \pi\rho \frac{N_A}{A} \frac{D_{\alpha-N}^2}{\theta_{\min}^2} t \approx 47500$ (2.88)

The radon-222  $\alpha$  particles allowed penetration of the atom but their energy was neither too large to cause nuclear penetration and associated nuclear reactions nor large enough to require relativistic treatment of the  $\alpha$ -particle velocity. Since artificial nuclear reactions and the relativistic mechanics were not understood in 1909 when the Geiger–Marsden experiment was carried out, Rutherford would not be able to solve with such elegance the atomic model question, if the kinetic energy of the  $\alpha$  particles used in the experiment was much larger than 5.5 MeV thereby causing penetration of the gold nucleus or much smaller than 5.5 MeV thereby preventing penetration of the atom.

Geiger–Marsden experiment provided the stimulus for development of nuclear physics and will remain forever on the short list of milestones in physics. It also served as the first known method for estimation of the upper limit of nuclear size through the calculation of the distance of closest approach  $D_{\alpha-N}$  but was soon eclipsed by new and more sophisticated scattering experiments that are now used for this purpose. However, the basic principles of the original technique are still used in the so-called Rutherford backscattering spectroscopy (RBS) which is an analytical tool used in materials science for determining structure and composition of materials by measuring backscattering of a beam of high energy ions (protons or helium ions) accelerated in a linear accelerator.

## 2.5 Mott Scattering

In comparison with heavy charged particles, energetic electrons are much better suited for studies of nuclear size and charge distribution. However, to obtain agreement with experimental results, the theoretical treatment of the scattering process must go beyond the rudimentary Rutherford-Coulomb point-source scattering approach and account for various other parameters such as:

1. Electron spin
2. Relativistic effects
3. Quantum effects
4. Recoil of the nucleus
5. Nuclear spin
6. Finite size of the nucleus

Accounting for these additional parameters refines the scattering theory beyond the level achieved by Rutherford but also makes it significantly more complex. For example, the finite size of the nucleus implies that the target is not a point charge but consists of its own structure containing protons and neutrons which, in turn, have their own constituents referred to as quarks.

At low electron energies where the electron does not penetrate the nucleus the electron scattering by the nucleus can be described with the standard Rutherford-type scattering formula [see (2.39)]

$$\frac{d\sigma_{\text{Ruth}}}{d\Omega} = \left(\frac{D_{e-N}}{4}\right)^2 \frac{1}{\sin^4 \frac{\theta}{2}} = \left(\frac{D_{e-N}}{2}\right)^2 \frac{1}{(1 - \cos \theta)^2} = \left(\frac{Z\alpha\hbar c}{4E_K}\right)^2 \frac{1}{\sin^4 \frac{\theta}{2}}, \quad (2.93)$$

where

$$D_{e-N} = \frac{Ze^2}{4\pi\epsilon_0 \frac{1}{2}mv^2} \quad (2.94)$$

is here referred to as the effective characteristic distance for the electron–nucleus scattering (see Sect. 2.6.2) in contrast to the distance of closest approach  $D_{\alpha-N}$  used in Rutherford scattering of  $\alpha$  particles, as discussed in Sect. 2.3.2. In the expression for  $D_{e-N}$  of (2.93),  $m$  is the total mass of the incident electron in contrast to  $m_e$  which is the rest mass of the electron ( $m = m_e/\sqrt{1 - (v/c)^2}$ ), and  $v$  is the velocity of the incident electron.

At very high electron energies (above 100 MeV) electrons are highly relativistic and two corrections to the simple Rutherford-type formula (2.93) are required: correction for electron spin and correction for nuclear recoil.

### 2.5.1 Correction for Electron Spin

The effect of the electron magnetic moment introduces to the Rutherford relationship for electron scattering given in (2.93) a spin correction factor expressed as

$$f_{\text{spin}} = 1 - \beta^2 \sin^2 \frac{\theta}{2}, \quad (2.95)$$

which, for relativistic electrons where  $\beta = v/c \rightarrow 1$ , simplifies to

$$f_{\text{spin}} \approx 1 - \sin^2 \frac{\theta}{2} = \cos^2 \frac{\theta}{2} = \frac{1 + \cos \theta}{2}. \quad (2.96)$$

For relativistic electrons ( $v \approx c$ ) the spin correction factor  $f_{\text{spin}}$  does not depend on the kinetic energy  $E_K$  of the incident electron but depends on the scattering angle  $\theta$  and, as shown in Fig. 2.7, ranges from  $f_{\text{spin}} = 1$  for  $\theta = 0$  through  $f_{\text{spin}} = 0.85$  for  $\theta = 45^\circ$ ,  $f_{\text{spin}} = 0.5$  for  $\theta = 90^\circ$  and  $f_{\text{spin}} = 0.146$  for  $\theta = 135^\circ$  to  $f_{\text{spin}} = 0$  for  $\theta = 180^\circ$ . Thus, at small scattering angles  $\theta$  the electron spin effects are negligible, while at large scattering angles they significantly decrease the differential scattering cross section from that given by the Rutherford expression of (2.93), essentially disallowing electron backscattering at  $\theta = 180^\circ$ .

Figure 2.8 plots, for a point-like Coulomb scattering source, the differential cross section for electron–nucleus scattering without spin correction in curve (1) and with spin correction in curve (2). The following expressions are plotted:

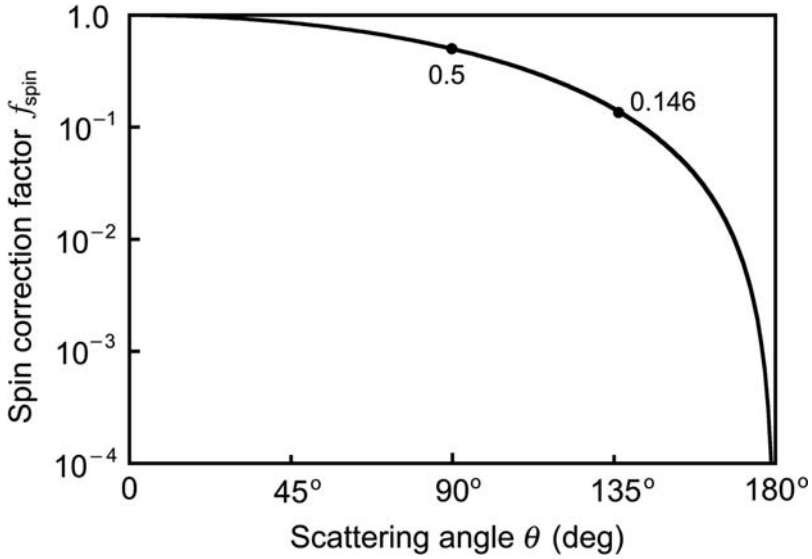


Fig. 2.7. Spin correction factor  $f_{\text{spin}}$  of (2.96) against scattering angle  $\theta$  for electron-nucleus (Mott) scattering

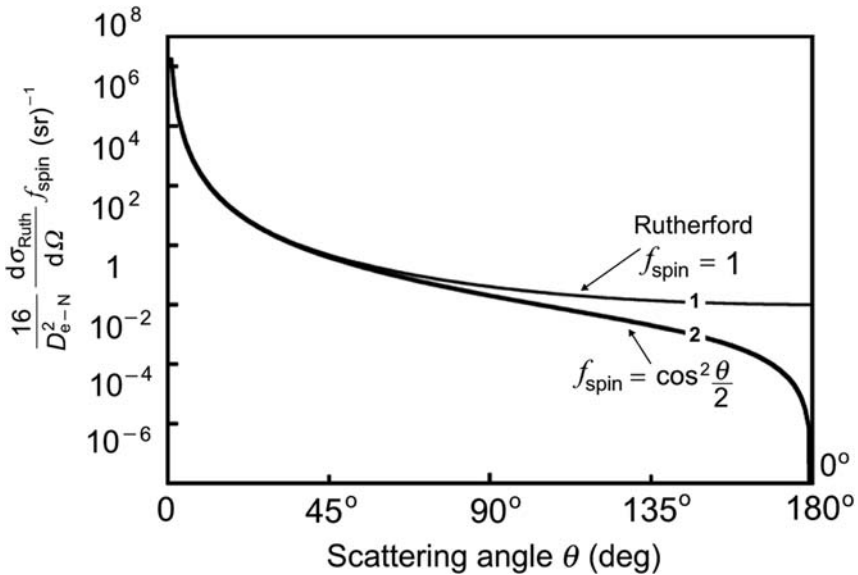


Fig. 2.8. Normalized Mott differential scattering cross section  $d\sigma_{\text{Mott}}/d\Omega$  against scattering angle  $\theta$ . Curve (1) is the Rutherford component without electron spin correction (i.e.,  $f_{\text{spin}} = 1$ ); curve (2) is for the Rutherford component corrected for the electron spin effect given as  $f_{\text{spin}} = \cos^2 \left(\frac{1}{2} \theta\right) = \frac{1}{2}(1 + \cos \theta)$

$$\frac{16}{D_{e-N}^2} \frac{d\sigma_{\text{Mott}}}{d\Omega} = \frac{16}{D_{e-N}^2} \frac{d\sigma_{\text{Ruth}}}{d\Omega} f_{\text{spin}} = \frac{1}{\sin^4 \frac{\theta}{2}} \times \frac{1 + \cos \theta}{2}, \quad (2.97)$$

where

- curve (1) is without spin correction or  $f_{\text{spin}} = 1$  independent of  $\theta$   
 curve (2) is with spin correction given in Fig. 2.7 and (2.96) as  $f_{\text{spin}} = \cos^2(\theta/2)$ .

### 2.5.2 Correction for Recoil of the Nucleus

The nuclear recoil correction factor  $f_{\text{recoil}}$  is given as the ratio between the kinetic energy of the scattered (recoil) electron  $E'_K$  and the kinetic energy of the incident electron  $E_K$ . The kinetic energy of the scattered electron  $E'_K$  is determined from considerations of conservation of energy and momentum during the scattering process. The considerations resemble the derivation of scattered photon energy and recoil electron kinetic energy in Compton effect (see Sect. 7.3.3).

The schematic diagram of the scattering process is shown in Fig. 2.9 where an incident electron with momentum  $\mathbf{p}$  and kinetic energy  $E_K$  is scattered, essentially elastically, through a scattering angle  $\theta$  to end with momentum  $\mathbf{p}'$  and kinetic energy  $E'_K$ . To be useful as a nuclear probe and to have a relatively small de Broglie wavelength (of the order of 10 fm) the electron must be of sufficiently high kinetic energy and is thus relativistic. The conservation of energy during the scattering process is written as follows

$$Mc^2 + E_K + m_e c^2 = \Delta E_K + Mc^2 + E'_K + m_e c^2 \quad (2.98)$$

or

$$E_K = \Delta E_K + E'_K, \quad (2.99)$$

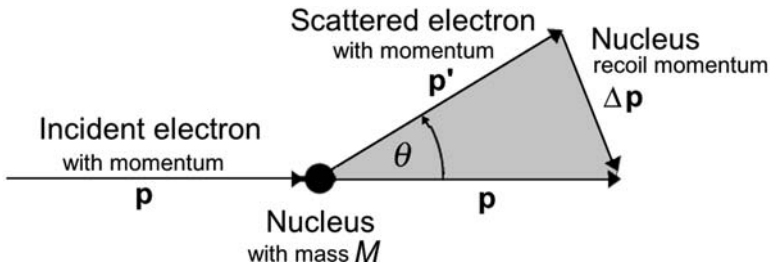


Fig. 2.9. Schematic representation of electron–nucleus (Mott) scattering

where

$\Delta E_K$  is the recoil kinetic energy transferred from the incident electron to the nucleus,

$Mc^2$  is the rest energy of the nucleus,

$m_e c^2$  is the rest energy of the incident electron.

Using the law of cosines on the vector diagram of Fig. 2.9, the conservation of momentum  $\mathbf{p} = \mathbf{p}' + \Delta\mathbf{p}$ , with an assumption that in elastic scattering  $|\mathbf{p}| \approx |\mathbf{p}'|$ , can be stated as follows

$$|\Delta\mathbf{p}|^2 = |\mathbf{p}|^2 + |\mathbf{p}'|^2 - 2|\mathbf{p}||\mathbf{p}'|\cos\theta \approx 2|\mathbf{p}|^2(1 - \cos\theta), \quad (2.100)$$

where  $\Delta\mathbf{p}$  is the recoil momentum of the nucleus. The recoil kinetic energy  $\Delta E_K$  is given as

$$\Delta E_K \approx \frac{|\Delta\mathbf{p}|^2}{2M} = \frac{|\mathbf{p}|^2(1 - \cos\theta)}{M} = \frac{E_K^2}{Mc^2} \left(1 + \frac{2m_e c^2}{E_K}\right) (1 - \cos\theta), \quad (2.101)$$

using the expression for the incident electron momentum magnitude  $|\mathbf{p}| = p$  of (1.64) given as

$$p = \frac{1}{c} \sqrt{E_K^2 + 2E_K m_e c^2} = \frac{E_K}{c} \sqrt{1 + \frac{2m_e c^2}{E_K}}. \quad (2.102)$$

Recognizing that in the electron scattering experiment  $m_e c^2 \ll E_K \ll Mc^2$  and  $E'_K = E_K - \Delta E_K$  we now get the following expression for the recoil correction  $f_{\text{recoil}}$

$$f_{\text{recoil}} = \frac{E'_K}{E_K} = \frac{1}{1 + \frac{E_K}{Mc^2}(1 - \cos\theta)} = \frac{1}{1 + \frac{2E_K}{Mc^2} \sin^2 \frac{\theta}{2}}. \quad (2.103)$$

The recoil correction factor  $f_{\text{recoil}}$  depends on the kinetic energy  $E_K$  of the incident electron, the rest mass of the scattering nucleus  $Mc^2$ , and the scattering angle  $\theta$ . For small scattering angles  $f_{\text{recoil}} \approx 1$  irrespective of  $E_K$  and then, for a given  $E_K/Mc^2$ , it decreases with  $\theta$  increasing from 0 to 180°. Since generally  $Mc^2 \gg E_K$ , unless we are dealing with very low atomic number scatterer and very high incident electron kinetic energy, it is reasonable to assume that  $f_{\text{recoil}} \approx 1$ .

Figure 2.10 plots the relationship between the kinetic energy of the scattered electron  $E'_K$  and the kinetic energy of the incident electron  $E_K$  for four scattering angles ( $0$ ,  $\frac{1}{4}\pi$ ,  $\frac{1}{2}\pi$ , and  $\pi$ ) of Mott scattering on hydrogen and gold nuclei in the kinetic energy range from 1 MeV to  $10^6$  MeV. In the electron kinetic energy of interest in medical physics (up to 30 MeV), the kinetic energy of the scattered electron  $E'_K$  is equal to the kinetic energy of

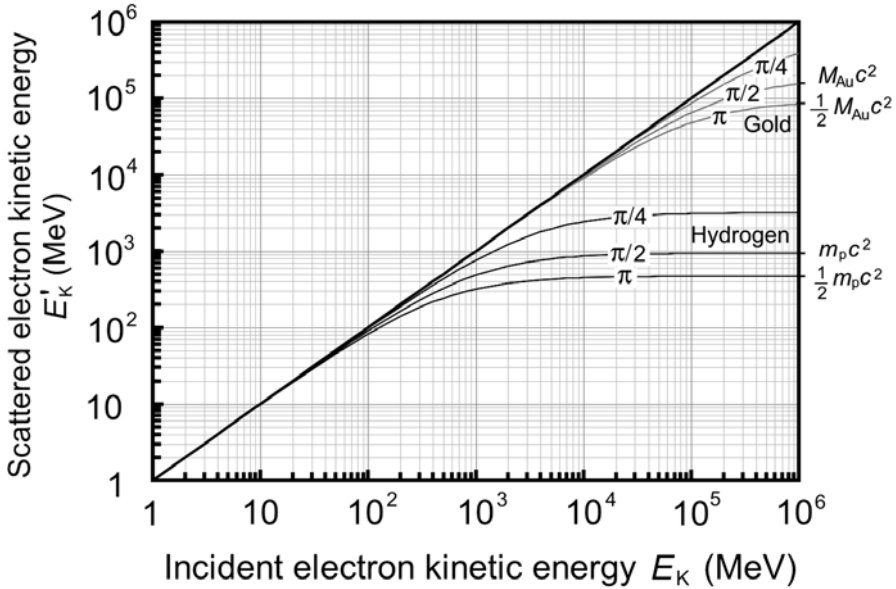


**Fig. 2.10.** Scattered electron kinetic energy  $E'_K = f_{\text{recoil}}E_K$  against the incident electron kinetic energy  $E_K$  for Mott scattering on hydrogen and gold nuclei for four different scattering angles ( $0, \frac{1}{4}\pi, \frac{1}{2}\pi,$  and  $\pi$ ). The recoil correction  $f_{\text{recoil}}$  is given in (2.103)

the incident electron  $E_K$  for all scattering materials and all scattering angles  $\theta$ . This implies that  $f_{\text{recoil}} = 1$  for all situations of interest in medical physics.

From Fig. 2.10 we arrive at several other conclusions, of little interest in medical physics but relevant to high energy physics:

1.  $f_{\text{recoil}} = 1$  for  $\theta = 0$  at all kinetic energies of the incident electron from 0 to  $\infty$ .
2. For backscattered electron ( $\theta = \pi$ ), its kinetic energy saturates at  $\frac{1}{2}Mc^2$  where  $M$  is the rest mass of the recoil nucleus. This results in  $f_{\text{recoil}} \rightarrow 0$  but happens only at very large incident electron kinetic energies, way outside of the energy region of interest in medical physics.
3. Similarly, for side-scattered electron ( $\theta = \frac{1}{2}\pi$ ), its kinetic energy saturates at  $Mc^2$  at very high incident electron kinetic energy.
4. The findings in points (2) and (3) are similar to relationships observed in Compton scattering (see Sect. 7.3.3) except that in Compton scattering the recoil particle is an electron which has a significantly smaller rest energy than a nucleus. This makes the recoil of the Compton electron of great importance to medical physics, since a significant fraction of the incident photon energy is transferred to the recoil electron in the photon energy range of interest in medical physics.

### 2.5.3 Differential Cross Section for Mott Scattering of Electrons on Point-Like Atomic Nuclei

Accounting for the spin correction of (2.96) and the nuclear recoil correction of (2.103) we now write the Mott expression for the differential cross section in electron–nucleus scattering as

$$\frac{d\sigma_{\text{Mott}}}{d\Omega} = \frac{d\sigma_{\text{Ruth}}}{d\Omega} f_{\text{spin}} f_{\text{recoil}} = \frac{d\sigma_{\text{Ruth}}}{d\Omega} \left\{ \cos^2 \frac{\theta}{2} \right\} \times \frac{1}{1 + \frac{E_K}{Mc^2} (1 - \cos \theta)}, \quad (2.104)$$

where  $d\sigma_{\text{Ruth}}/d\Omega$  is the Rutherford electron–nucleus scattering formula given in (2.93) and valid at very low electron kinetic energies. The most important component of (2.104) is the Rutherford component; the product of the two corrections to the Rutherford component (the electron spin quantum effect  $f_{\text{spin}}$  and the nuclear recoil  $f_{\text{recoil}}$ ) is of the order of unity except when the scattering angle  $\theta$  is close to  $180^\circ$  or when the kinetic energy of the incident electron is very large.

### 2.5.4 Hofstadter Correction for Finite Nuclear Size and the Form Factor

Figure 2.11 shows, for scattering of 125 MeV electrons on gold nuclei, several differential cross sections plotted against the scattering angle  $\theta$ :

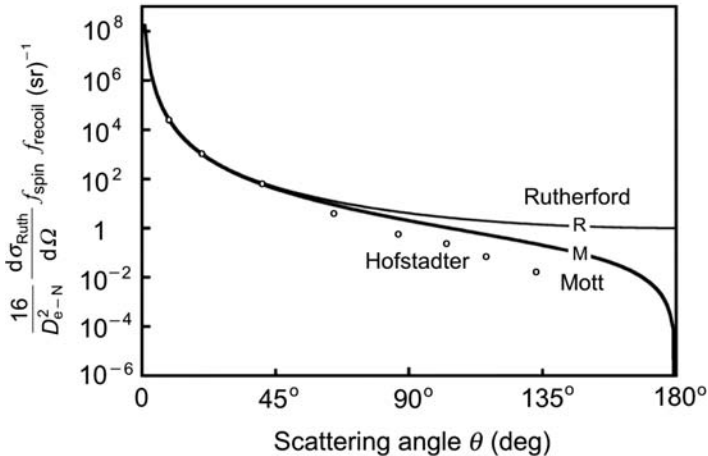


**Fig. 2.11.** Elastic scattering of 125 MeV electrons on gold nuclei. Curve (R) is for data calculated with Rutherford equation (2.93) without spin or nuclear recoil correction. Curve (M) is for Rutherford equation incorporating spin correction of (2.96) and nuclear recoil correction of (2.103). Data points are Hofstadter’s measured data

1. Curve (R) represents the calculated simple Rutherford differential cross section (2.93) assuming a point-like Coulomb field and ignoring the electron spin effects as well as nuclear recoil.
2. Curve (M) represents the Mott differential scattering cross section (2.104) assuming a point-like Coulomb source and incorporating corrections for electron spin ( $f_{\text{spin}}$ ) and nuclear recoil ( $f_{\text{recoil}} \approx 1$ ).
3. Data points represent data that *Robert Hofstadter* measured in the early 1960s at Stanford University. While at small scattering angles Hofstadter's measurements agree with the Mott theory, for scattering angles  $\theta$  exceeding  $45^\circ$  the measured points show significantly lower values than the theory, and the discrepancy increases with increasing  $\theta$ .

Hofstadter carried out extensive experimental and theoretical studies of electron–nucleus scattering and for this work received a Nobel Prize in Physics in 1961. He explained the discrepancy between his measured data and Mott theory of Fig. 2.11 by expanding the Mott expression of (2.104) to account for the finite size of the nucleus using a form factor  $F(K)$  correction. The experimental differential cross section for elastic electron–nucleus scattering then becomes expressed as

$$\frac{d\sigma_{\text{exp}}}{d\Omega} = \frac{d\sigma_{\text{Mott}}}{d\Omega} |F(K)|^2 = \frac{d\sigma_{\text{Ruth}}}{d\Omega} \left\{ \cos^2 \frac{\theta}{2} \right\} \times \frac{1}{1 + \frac{E_K}{Mc^2} (1 - \cos \theta)} |F(K)|^2, \quad (2.105)$$

where  $K$  is proportional to the momentum transferred from incident electron to the nucleus, or

$$K = |\mathbf{K}| = \frac{1}{\hbar} \sqrt{|\mathbf{p}_i|^2 + |\mathbf{p}_f|^2 - 2|\mathbf{p}_i||\mathbf{p}_f| \cos \theta} = \frac{1}{\hbar} 2p \sin \frac{\theta}{2} = \frac{2}{\lambda} \sin \frac{\theta}{2}. \quad (2.106)$$

The form factor  $F(K)$  represents a Fourier transform of the nuclear charge density distribution  $\rho(r)$  assumed to be spherically symmetric. In the Born approximation (see Sect. 1.23.6),  $F(K)$  is expressed as

$$\begin{aligned} F(K) &= \iiint \rho(r) e^{i\mathbf{K}\mathbf{r}} dV = \int_0^\infty \int_0^\pi \int_0^{2\pi} \rho(r) e^{iKr \cos \theta} r^2 dr \sin \theta d\theta d\phi \\ &= 2\pi \int_0^\infty r^2 \rho(r) \left\{ \int_{-1}^1 e^{iKr \cos \theta} d(\cos \theta) \right\} dr \\ &= 2\pi \int_0^\infty r^2 \rho(r) \frac{e^{iKr} - e^{-iKr}}{iKr} dr = 2\pi \int_0^\infty r^2 \rho(r) \frac{\sin Kr}{Kr} dr, \quad (2.107) \end{aligned}$$

with the normalization

$$\int \rho(r) d\mathcal{V} = \int_0^\infty \int_{-1}^{+1} \int_0^{2\pi} r^2 \rho(r) d\phi d(\cos \theta) dr = 4\pi \int_0^\infty \rho(r) r^2 dr = 1. \quad (2.108)$$

The magnitude of the form factor  $F(K)$  is determined experimentally by comparing the measured cross section to the Mott cross section for point-like nucleus. The measurements are carried out for fixed electron beam energy at various scattering angles  $\theta$ , i.e., at various values of  $|\mathbf{K}| = K$ . In practice, however,  $F(K)$  can be measured only over a limited range of momentum transfer  $|\mathbf{K}|/\hbar$  so that a full functional dependence of  $F(K)$  cannot be determined for use in inverse Fourier transform which would yield the nuclear charge distribution  $\rho(r)$

$$\rho(r) = \frac{1}{(2\pi)^3} \int F(K) e^{-i\mathbf{K}\mathbf{r}} d\mathcal{V}. \quad (2.109)$$

Much effort has been spent on experimental determination of nuclear size and charge distribution. The current consensus is that nuclei are not charged spheres with a sharply defined surface. Rather, the nuclear charge density  $\rho(r)$  can be described by a Fermi function with two parameters ( $\alpha$  and  $\beta$ ) both of the order of 1 fm

$$\rho(r) = \frac{\rho(0)}{1 + e^{(r-\alpha)/\beta}}. \quad (2.110)$$

As a guide to nuclear size, the nucleus is commonly approximated as a homogeneously charged sphere with radius  $R$  given as

$$R = R_0 \sqrt[3]{A}, \quad (2.111)$$

where  $A$  is the atomic mass number and  $R_0$  is the nuclear radius constant amounting to 1.25 fm, as discussed in Sect. 1.16.1.

## 2.6 General Aspects of Elastic Scattering of Charged Particles

Most interactions of energetic charged particles as they traverse an absorber can be characterized as elastic Coulomb scattering between an energetic charged particle and the atoms of the absorber. The charged particles of interest in medical physics are either light charged particles such as electrons and positrons or heavy charged particles such as protons,  $\alpha$  particles, and heavier ions. Negative pions  $\pi^-$  were included in the group of charged particles as intermediate mass particles; however, interest in their use in radiotherapy has waned during the past 20 years with the advent of proton radiotherapy machines.

Charged particles can have elastic scattering interactions with orbital electrons as well as nuclei of the absorber atoms. The Coulomb force between the charged particle and the orbital electron or the nucleus of the absorber governs the elastic collisions and is either attractive or repulsive depending on the polarity of the interacting charged particles. In either case the trajectory of the projectile is a hyperbola: for an attractive Coulomb force the target is in the inner focus of the hyperbola; for a repulsive Coulomb force the target is in the outer focus of the hyperbola. An elastic collision between an  $\alpha$  particle and a nucleus of an absorber is shown schematically in Fig. 2.3 (Rutherford scattering) in Sect. 2.3.1; an elastic collision between a heavy charged particle and an orbital electron is shown schematically in Fig. 6.3 in Sect. 6.4.1.

Various investigators worked on theoretical aspects of elastic scattering of charged particles, most notably: *Rutherford* with *Geiger* and *Marsden* on  $\alpha$  particle scattering; *Mott* on electron–nucleus scattering as well as on non-relativistic electron–orbital electron scattering; *Møller* on relativistic electron–orbital electron scattering; *Bhabha* on positron–orbital electron scattering; and *Molière* on multiple scattering.

As shown in previous sections of this chapter, Rutherford scattering theory forms the basis for all charged particle single scattering theories. However, various corrections must be applied to Rutherford’s formalism when moving from a discussion of classical  $\alpha$  particle scattering on an infinite-mass gold nucleus to a discussion of relativistic electrons scattered on finite size absorber nuclei. To highlight the various different projectiles, scattering centers, and corrections, in addition to Rutherford scattering, we speak of Mott scattering, Møller scattering, Bhabha scattering, Hofstadter scattering, etc in single scattering events and of Molière scattering when we consider the composite effect of scattering on a large number of scattering centers.

The particle interactions in absorbers are characterized by various parameters that describe single and multiple scattering events:

1. For *single scattering* we define the differential and total scattering cross section, effective characteristic distance, and mean square scattering angle.
2. For *multiple scattering* we define the mean square scattering angle and the mass scattering power.

### 2.6.1 Differential Scattering Cross Section for a Single Scattering Event

The differential scattering cross section  $d\sigma/d\Omega$  for a single scattering event between two charged particles was discussed in relation to Rutherford scattering in Sect. 2.3. In the small scattering angle  $\theta$  approximation where  $\sin(\frac{1}{2}\theta) \approx \frac{1}{2}\theta$ , the differential scattering cross section based on Rutherford’s

seminal work is in general expressed as

$$\frac{d\sigma}{d\Omega} = \frac{D^2}{(\theta^2 + \theta_{\min}^2)^2}, \quad (2.112)$$

where  $\theta_{\min}$  is a cutoff angle; a minimum angle below which the unscreened point Coulomb field expression is no longer valid;  $D$  is a scattering parameter generally referred to as the *characteristic scattering distance*, such as, for example,  $D_{\alpha-N}$  defined as the distance of closest approach between the  $\alpha$  particle and the nucleus in Rutherford scattering.

### 2.6.2 Characteristic Scattering Distance

Each elastic scattering event between two particles (energetic projectile and stationary target) can be characterized by a scattering parameter referred to as the characteristic scattering distance  $D$ . This distance depends on the nature of the specific scattering event as well as on the physical properties of the scattered particle and the atomic number  $Z$  of the scattering material. The differential scattering cross section of (2.38) was derived for Rutherford scattering of  $\alpha$  particles on gold nuclei in Sect. 2.4.1 and is a good approximation for scattering of both heavy and light charged particles, as long as the characteristic scattering distance  $D$ , appropriate for the particular scattering event, is used in the calculations.

#### Characteristic Scattering Distance for Rutherford Scattering

In *Rutherford scattering* of a  $\alpha$  particle (projectile) on a nucleus (target) the characteristic scattering distance  $D$ , as shown in (2.12) and (2.30), is the distance of closest approach  $D_{\alpha-N}$  between the  $\alpha$  particle and the nucleus in a direct-hit (head on) collision ( $b = 0$ ,  $\theta = \pi$ )

$$D_{\alpha-N} = \frac{zZe^2}{4\pi\epsilon_0} \frac{1}{(E_K)_i} = \frac{zZe^2}{4\pi\epsilon_0} \frac{1}{\frac{m_\alpha v_\alpha^2}{2}} = \frac{2zZe^2}{4\pi\epsilon_0} \frac{1}{p_\alpha v_\alpha}, \quad (2.113)$$

where

- $z$  is the atomic number of the  $\alpha$  particle,
- $Z$  is the atomic number of the absorber atom,
- $(E_K)_i$  is the initial kinetic energy of the  $\alpha$  particle,
- $m_\alpha$  is the mass of the  $\alpha$  particle,
- $v_\alpha$  is the initial and final velocity of the  $\alpha$  particle,
- $p_\alpha$  is the momentum of the  $\alpha$  particle

### Characteristic Scattering Distance for Electron–Nucleus Scattering

In *electron* (projectile)–*nucleus* (target) *elastic scattering* the characteristic scattering distance  $D_{e-N}$ , similarly to (2.113), is given as follows (note that  $z = 1$  for the electron)

$$D_{e-N} = \frac{Ze^2}{4\pi\epsilon_0} \frac{1}{\frac{mv^2}{2}} = \frac{2Ze^2}{4\pi\epsilon_0} \frac{1}{pv} = \frac{2Ze^2\sqrt{1-\beta^2}}{4\pi\epsilon_0(m_e c^2 \beta^2)} = \frac{2Zr_e\sqrt{1-\beta^2}}{\beta^2}, \quad (2.114)$$

where

- $m$  is the total mass of the electron, i.e.,  $m = m_e/\sqrt{1-\beta^2} = \gamma m_e c^2$ .
- $m_e$  is the rest mass of the electron.
- $\beta$  is the velocity of the electron normalized to  $c$ , i.e.,  $\beta = v/c$ .
- $v$  is the velocity of the electron.
- $p$  is the momentum of the electron.
- $Z$  is the atomic number of the absorber.
- $r_e$  is the classical radius of the electron (2.82 fm).

### Characteristic Scattering Distance for Electron–Orbital Electron Scattering

In *electron* (projectile)–*orbital electron* (target) *scattering* the characteristic scattering distance  $D_{e-e}$ , similarly to (2.114), is given by (note that  $Z = 1$  for orbital electron)

$$D_{e-e} = \frac{e^2}{4\pi\epsilon_0} \frac{1}{\frac{mv^2}{2}} = \frac{2e^2}{4\pi\epsilon_0} \frac{1}{pv} = \frac{2e^2\sqrt{1-\beta^2}}{4\pi\epsilon_0(m_e c^2 \beta^2)} = \frac{2r_e\sqrt{1-\beta^2}}{\beta^2}, \quad (2.115)$$

where

- $m$  is the *total mass* of the electron, i.e.,  $m = m_e/\sqrt{1-\beta^2} = \gamma m_e c^2$ .
- $m_e$  is the rest mass of the electron.
- $\beta$  is the velocity of the electron normalized to  $c$ , i.e.,  $\beta = v/c$ .
- $v$  is the velocity of the electron.
- $p$  is the momentum of the electron.
- $r_e$  is the classical radius of the electron (2.82 fm).

### Characteristic Scattering Distance for Electron–Atom Scattering

The *characteristic scattering distance*  $D_{e-a}$  for electron (projectile) scattering on absorber atoms (target) has two components: the *electron–nucleus* (e–N) component of (2.114) and the *electron–orbital electron* (e–e) component of

(2.115). The differential cross section for elastic electron scattering on atoms of an absorber consists of the sum of the differential electron–nucleus cross section and  $Z$  times the differential electron–orbital electron cross section, i.e.,

$$\left. \frac{d\sigma}{d\Omega} \right|_{e-a} = \left. \frac{d\sigma}{d\Omega} \right|_{e-N} + Z \left. \frac{d\sigma}{d\Omega} \right|_{e-e} = \frac{D_{e-a}^2}{(\theta^2 + \theta_{\min}^2)^2}, \quad (2.116)$$

where  $D_{e-a}$  is the characteristic scattering distance for *electron-atom* elastic scattering given as

$$D_{e-a}^2 = D_{e-N}^2 + Z D_{e-e}^2. \quad (2.117)$$

The characteristic scattering distance  $D_{e-a}$  is determined from (2.117) after inserting (2.114) and (2.115) to get

$$\begin{aligned} D_{e-a} &= \sqrt{D_{e-N}^2 + Z D_{e-e}^2} = \frac{e^2}{4\pi\epsilon_0} \frac{\sqrt{Z(Z+1)}}{\frac{mv^2}{2}} = \frac{2e^2}{4\pi\epsilon_0} \frac{\sqrt{Z(Z+1)}}{pv} \\ &= \frac{2r_e \sqrt{Z(Z+1)} \sqrt{1-\beta^2}}{\beta^2} = \frac{2r_e \sqrt{Z(Z+1)}}{\gamma\beta^2}, \end{aligned} \quad (2.118)$$

where

- $m$  is the *total mass* of the electron, i.e.,  $m = m_e/\sqrt{1-\beta^2} = \gamma m_e c^2$ .
- $m_e$  is the rest mass of the electron.
- $\beta$  is the velocity of the electron normalized to  $c$ , i.e.,  $\beta = v_e/c$ .
- $v_e$  is the velocity of the electron.
- $p$  is the momentum of the electron.
- $Z$  is the atomic number of the absorber.
- $r_e$  is the classical radius of the electron (2.82 fm).

A summary of characteristic scattering distances  $D$  for four elastic Coulomb scattering events including scattering of: (1)  $\alpha$  particle on nucleus (Rutherford scattering); (2) electron on nucleus (Mott scattering); (3) electron on atomic orbital electron; and (4) electron on atom is given in Table 2.4.

### 2.6.3 Minimum and Maximum Scattering Angles

The minimum and maximum scattering angles  $\theta_{\min}$  and  $\theta_{\max}$ , respectively, are angles where the deviation from point Coulomb nuclear field becomes significant. These departures from the point Coulomb field approximation appear at very small and very large scattering angles  $\theta$ , corresponding to very large and very small impact parameters  $b$ , respectively.

At very small angles  $\theta$  the screening of the nuclear charge by atomic orbital electrons decreases the differential cross section and at large angles  $\theta$  the finite nuclear size or nuclear penetration by the charged particle decreases the differential cross section, as discussed for Rutherford scattering in Sects. 2.4.4 and 2.4.6, respectively.

**Table 2.4.** Characteristic scattering distances  $D$  for four elastic Coulomb scattering events. Note that  $m$  in  $D_{e-N}$ ,  $D_{e-e}$ , and  $D_{e-a}$  stands for the **total mass** of the electron and not the rest mass of the electron

Elastic Coulomb scattering	Characteristic scattering distance $D$	
$\alpha$ Particle–nucleus (Rutherford)	$D_{\alpha-N} = \frac{zZe^2}{4\pi\epsilon_0 \frac{m_\alpha v_\alpha^2}{2}} = \frac{zZe^2}{4\pi\epsilon_0 (E_K)_i}$	See (2.12) and (2.113)
Electron–nucleus (Mott)	$D_{e-N} = \frac{Ze^2}{4\pi\epsilon_0 \frac{mv_e^2}{2}} = \frac{2Zr_e\sqrt{1-\beta^2}}{\beta^2}$	See (2.94) and (2.114)
Electron–orbital electron	$D_{e-e} = \frac{e^2}{4\pi\epsilon_0 \frac{mv_e^2}{2}} = \frac{2r_e\sqrt{1-\beta^2}}{\beta^2}$	See (2.115)
Electron–atom	$D_{e-a} = \frac{e^2\sqrt{Z(Z+1)}}{4\pi\epsilon_0 \frac{mv_e^2}{2}} = \frac{2r_e\sqrt{Z(Z+1)}\sqrt{1-\beta^2}}{\beta^2}$	See (2.116)

As evident from Figs. 2.3 and 6.3, the relationship governing the change of momentum  $\Delta p$  in elastic scattering is given as follows

$$\sin \frac{\theta}{2} = \frac{\Delta p}{p_i}, \tag{2.119}$$

where

- $\theta$  is the scattering angle,
- $p_i$  is the particle initial momentum at a large distance from the scattering interaction.

In the small angle  $\theta$  approximation, we get the following simple relationship from (2.22) and (2.119) recognizing that  $\sin \theta \approx \theta$

$$\theta \approx \frac{\Delta p}{p_i}. \tag{2.120}$$

As shown in (2.57) and (2.69),  $\theta_{\min}$  and  $\theta_{\max}$ , respectively, are given by the following quantum-mechanical expressions

$$\begin{aligned} \theta_{\min} &\approx \frac{\Delta p}{p_i} \approx \frac{\hbar}{a_{TF} p_i} = \frac{\hbar}{p_i} \frac{\sqrt[3]{Z}}{a_0} = \frac{\hbar c}{a_0} \frac{\sqrt[3]{Z}}{\sqrt{E_K(E_K + 2E_0)}} \\ &\approx \frac{3.723 \times 10^{-3} \text{ MeV} \sqrt[3]{Z}}{\sqrt{E_K(E_K + 2E_0)}} \end{aligned} \tag{2.121}$$

and

$$\begin{aligned}\theta_{\max} &\approx \frac{\Delta p}{p_i} \approx \frac{\hbar}{Rp_i} = \frac{\hbar}{p_i R_0 \sqrt[3]{A}} = \frac{\hbar c}{R_0 \sqrt[3]{A} \sqrt{E_K(E_K + 2E_0)}} \\ &\approx \frac{1.578 \times 10^2 \text{ MeV}}{\sqrt[3]{A} \sqrt{E_K(E_K + 2E_0)}},\end{aligned}\quad (2.122)$$

where

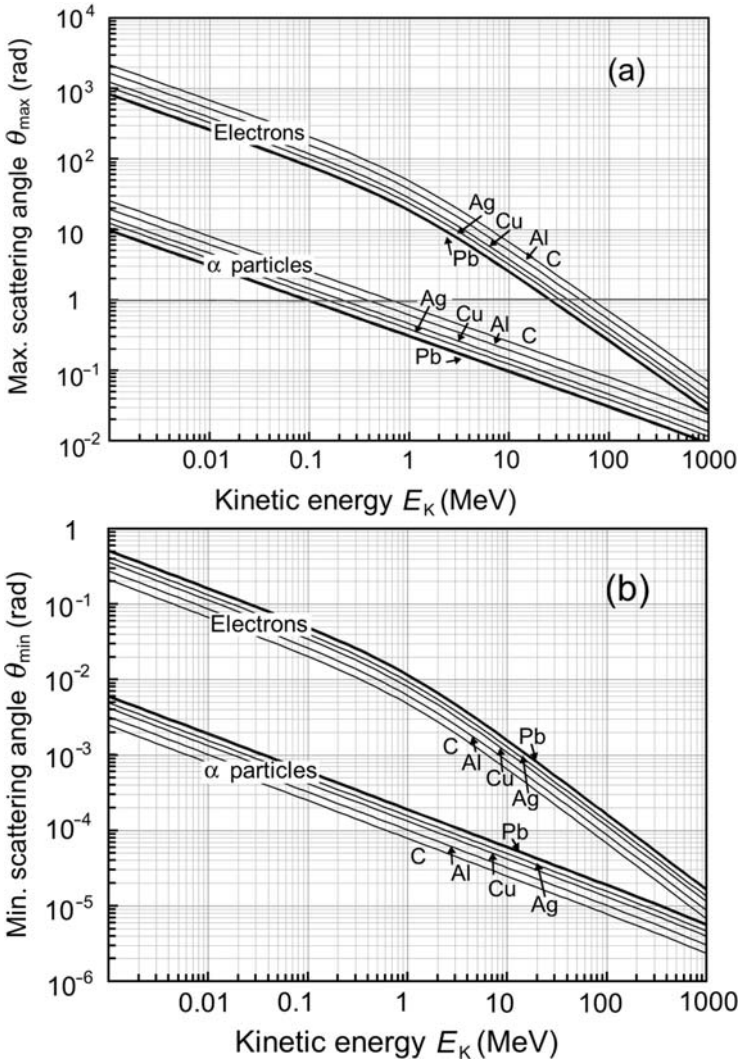
- $p_i$  is the initial momentum of the charged particle.
- $a_{\text{TF}}$  is the Thomas–Fermi atomic radius equal to  $\sim a_0 Z^{-1/3}$  with  $a_0$  the Bohr radius constant and  $Z$  the atomic number of the absorber, as given in (2.49).
- $a_0$  is the Bohr radius constant defined in (3.4).
- $R$  is the radius of the nucleus equal to  $R_0 A^{1/3}$  with  $R_0$  the nuclear radius constant ( $R_0 = 1.25 \text{ fm}$ ), as discussed in Sect. 1.16.1.
- $E_K$  is the initial kinetic energy of the charged particle related to the initial momentum of the charged particle through (1.64).
- $E_0$  is the rest energy of the charged particle.
- $A$  is the atomic mass number of the absorber.

Figure 2.12a shows the maximum scattering angle  $\theta_{\max}$  against kinetic energy  $E_K$  given in (2.122) in the range from 1 keV to 1000 MeV for electron and  $\alpha$  particle elastic scattering in carbon, aluminum, copper, silver, and lead. Figure 2.12b shows the minimum scattering angle  $\theta_{\min}$  given in (2.121) under same conditions as those in Fig. 2.12a. Based on (2.121) and (2.122) as well as Fig. 2.12 we now make the following observations about the minimum and maximum scattering angles  $\theta_{\min}$  and  $\theta_{\max}$ , respectively:

1. In general,  $\theta_{\min}$  and  $\theta_{\max}$  depend on the kinetic energy  $E_K$  and rest energy  $E_0$  of the elastically scattered projectile as well as the atomic number  $Z$  and atomic mass number  $A$  of the target. However, the ratio  $\theta_{\max}/\theta_{\min}$  is independent of the incident particle physical properties and depends solely on the atomic number  $Z$  and the atomic mass  $A$  of the absorber target as follows

$$\frac{\theta_{\max}}{\theta_{\min}} = \frac{a_0}{R_0 \sqrt[3]{A} \sqrt[3]{Z}} \approx \frac{0.5292 \text{ \AA}}{1.25 \times 10^{-5} \text{ \AA} \sqrt[3]{AZ}} \approx \frac{0.423 \times 10^5}{(AZ)^{1/3}} = \frac{\text{Const}}{\sqrt[3]{AZ}}. \quad (2.123)$$

2. For a given  $E_K$  the maximum scattering angle  $\theta_{\max}$  is inversely proportional to  $Z^{1/3}$  since  $\theta_{\max} \propto A^{-1/3}$  and  $A \approx 2Z$  and the minimum scattering angle  $\theta_{\min}$  is proportional to  $Z^{1/3}$ .
3. For kinetic energies  $E_K$  of the projectile much smaller than its rest energy  $E_0$ , or  $E_K \ll E_0$ , both  $\theta_{\min}$  and  $\theta_{\max}$  for a given target are proportional to  $1/\sqrt{E_K}$ , as shown in Fig. 2.12 in the whole  $E_K$  energy range for  $\alpha$  particles and at kinetic energies  $E_K$  below 100 keV for electrons.



**Fig. 2.12.** Maximum scattering angle  $\theta_{\max}$  in (a) and minimum scattering angle  $\theta_{\min}$  in (b) against kinetic energy  $E_K$  for electrons and  $\alpha$  particles scattered on carbon, aluminum, copper, silver, and gold

4. For kinetic energies  $E_K$  of the projectile much larger than its rest energy  $E_0$ , or  $E_K \gg E_0$ , both  $\theta_{\min}$  and  $\theta_{\max}$  for a given target are proportional to  $1/E_K$ , as shown in Fig. 2.12 for electrons in the energy range above 10 MeV.
5. For Rutherford scattering of 5.5 MeV  $\alpha$  particles on gold nucleus Au-197 (Geiger–Marsden experiment) we obtain from (2.121) a minimum scattering angle  $\theta_{\min}$  of  $8.1 \times 10^{-5}$  rad, as given in (2.72), and from (2.122) a maximum scattering angle of  $\theta_{\max}$  of 0.14 rad, as given in (2.73), in agreement with the general condition that  $\theta_{\min} \ll \theta_{\max} \ll 1$ .

6. For 10 MeV electrons scattered on gold-197, on the other hand, we find significantly larger  $\theta_{\min}$  from (2.121) and  $\theta_{\max}$  from (2.122) at  $1.5 \times 10^{-3}$  rad and 2.6 rad, respectively. However, we may still assume that  $\theta_{\min} \ll \theta_{\max}$ . Note: For  $\theta_{\max}$  calculated from (2.122) larger than unity,  $\theta_{\max}$  is usually set equal to 1.
7. The factor  $(AZ)^{1/3}$  ranges from unity for hydrogen to  $\sim 28$  for high atomic number absorbers such as uranium with  $Z = 92$  and  $A = 235$ .

### 2.6.4 Total Cross Section for a Single Scattering Event

The total cross section  $\sigma$  for a single scattering event, similarly to the discussion of Rutherford cross section given in Sect. 2.4.8, is approximated as follows using the small angle approximation  $\sin \theta \approx \theta$ :

$$\begin{aligned}
 \sigma &= \int \frac{d\sigma}{d\Omega} d\Omega \approx 2\pi D^2 \int_0^{\theta_{\max}} \frac{\theta d\theta}{(\theta^2 + \theta_{\min}^2)^2} = \pi D^2 \int_0^{\theta_{\max}} \frac{d(\theta^2 + \theta_{\min}^2)}{(\theta^2 + \theta_{\min}^2)^2} \\
 &= -\pi D^2 \left[ \frac{1}{\theta^2 + \theta_{\min}^2} \right]_0^{\theta_{\max}} = \pi D^2 \left\{ \frac{1}{\theta_{\min}^2} - \frac{1}{\theta_{\max}^2 + \theta_{\min}^2} \right\} \\
 &= \pi D^2 \frac{1}{\theta_{\min}^2} \left\{ 1 - \frac{1}{1 + (\theta_{\max}/\theta_{\min})^2} \right\}. \tag{2.124}
 \end{aligned}$$

Since  $\theta_{\max}/\theta_{\min} \gg 1$  even for very high atomic number materials, we can simplify the expression for total cross section  $\sigma$  to read

$$\sigma \approx \frac{\pi D^2}{\theta_{\min}^2}, \tag{2.125}$$

where

$D$  is the effective characteristic distance discussed in Sect. 2.6.2,  
 $\theta_{\min}$  is the minimum scattering angle discussed in Sect. 2.6.3.

### 2.6.5 Mean Square Scattering Angle for a Single Scattering Event

The mean square scattering angle for a single scattering event  $\overline{\theta^2}$  is defined by the following general relationship

$$\overline{\theta^2} = \frac{\int_0^{\theta_{\max}} \theta^2 \frac{d\sigma}{d\Omega} d\Omega}{\int_0^{\theta_{\max}} \frac{d\sigma}{d\Omega} d\Omega} = \frac{2\pi}{\sigma} \int_0^{\theta_{\max}} \theta^2 \frac{d\sigma}{d\Omega} \sin \theta d\theta, \tag{2.126}$$

where

- $d\sigma/d\Omega$  is the differential cross section for the single scattering event, given in (2.112),  
 $\sigma$  is the total cross section for the single scattering event [see (2.124) and (2.125)],  
 $\theta$  is the scattering angle for the single scattering event,  
 $\theta_{\max}$  is the maximum scattering angle calculated from (2.122). It is taken as the actual calculated value when the calculated  $\theta_{\max}$  is smaller than 1 and is taken as unity when the calculated  $\theta_{\max}$  exceeds 1.

The mean square angle  $\overline{\theta^2}$  for a single scattering event may be approximated in the small angle approximation as follows

$$\begin{aligned} \overline{\theta^2} &= \frac{2\pi D^2}{\sigma} \int_0^{\theta_{\max}} \frac{\theta^3 d\theta}{(\theta^2 + \theta_{\min}^2)^2} = \frac{\pi D^2}{\sigma} \int_0^{\theta_{\max}} \frac{(\theta^2 + \theta_{\min}^2) d(\theta^2 + \theta_{\min}^2)}{(\theta^2 + \theta_{\min}^2)^2} \\ &\quad - \frac{\pi D^2}{\sigma} \int_0^{\theta_{\max}} \frac{\theta_{\min}^2 d(\theta^2 + \theta_{\min}^2)}{(\theta^2 + \theta_{\min}^2)^2} \\ &= \frac{\pi D^2}{\sigma} \left\{ \ln \left( 1 + \frac{\theta_{\max}^2}{\theta_{\min}^2} \right) - \frac{1}{1 + (\theta_{\min}/\theta_{\max})^2} \right\} \end{aligned} \quad (2.127)$$

or, after inserting the expression for  $\sigma$  given in (2.125)

$$\begin{aligned} \overline{\theta^2} &= \theta_{\min}^2 \left\{ \ln \left( 1 + \frac{\theta_{\max}^2}{\theta_{\min}^2} \right) - \frac{1}{1 + (\theta_{\min}/\theta_{\max})^2} \right\} \\ &= \theta_{\min}^2 \ln \left( 1 + \frac{\theta_{\max}^2}{\theta_{\min}^2} \right) - \frac{\theta_{\min}^2 \theta_{\max}^2}{\theta_{\min}^2 + \theta_{\max}^2}. \end{aligned} \quad (2.128)$$

with  $\theta_{\min}$  minimum scattering angle defined in (2.121) and  $\theta_{\max}$  largest angle to be still considered a small angle in single scattering and defined in (2.122). At low energies  $\theta_{\max}$  calculated from (2.122) may exceed 1 rad and the maximum scattering angle is then taken as  $\theta_{\max} \approx 1$  rad.

The ratio  $\theta_{\max}/\theta_{\min}$  is independent of particle kinetic and total energy and depends only on the atomic number  $Z$  and the atomic mass number  $A$  of the absorber, as shown in (2.123). Since, in addition  $\theta_{\max} \gg \theta_{\min}$ , we can simplify (2.128) to read

$$\overline{\theta^2} \approx 2\theta_{\min}^2 \ln \frac{\theta_{\max}}{\theta_{\min}}. \quad (2.129)$$

After inserting (2.123) into (2.129) and assuming that  $A \approx 2Z$  we get the following approximation for the mean square scattering angle  $\overline{\theta^2}$  for single scattering

$$\overline{\theta^2} \approx 2\theta_{\min}^2 \ln \left( \frac{\sqrt{0.423 \times 10^5}}{\sqrt{\sqrt[3]{2} \sqrt[3]{Z}}} \right)^2 = 4\theta_{\min}^2 \ln [183Z^{-1/3}], \quad (2.130)$$

with the minimum scattering angle  $\theta_{\min}$  given in (2.121).

## 2.7 Molière Multiple Elastic Scattering

Multiple or compound Coulomb scattering results from a large number of single scattering events that a charged particle will experience as it moves through an absorber. These single scattering events are independent and statistically random processes governed by a Rutherford-type Coulomb interaction and confined to a very small scattering angle  $\theta$  with respect to the direction of incidence. In honor of Molière who carried out much of the initial theoretical work on multiple scattering, this type of scattering is often referred to as Molière multiple scattering.

As discussed for standard Rutherford scattering in Sect. 2.3, a particle traversing a thin metallic foil will experience a large number of Coulomb interactions with nuclei of the absorber and these interactions will generally produce only small angle deflections. The cumulative effect of these independent interactions will be a superposition of a large number of random deflections resulting in the particle emerging through the foil: (1) at a small cumulative scattering angle  $\Theta$ , and (2) at a mean scattering angle  $\overline{\Theta}$  with respect to the incident direction of zero for a beam of particles striking the foil.

The angular distribution of particles transmitted through a foil is Gaussian in shape and centered round the direction of the incident particles, reflecting the cumulative action of a large number of independent small-angle scattering interactions. This was shown by (2.2) for  $\alpha$ -particle scattering on gold nuclei.

The measured angular distributions of charged particles emerging through a foil show excellent agreement with a Gaussian distribution at small cumulative scattering angles  $\Theta$  but also exhibit a higher tail than the Gaussian distribution at large scattering angles. This discrepancy at large scattering angles is attributed to the effect of rare large-angle single scattering events which were first explained by Rutherford as follows: In its travel through the foil a charged particle may experience a close encounter with a scattering center and this hard collision will result in a large angle deflection, possibly amounting to  $180^\circ$ . These large-angle Coulomb scattering interactions are extremely rare yet not negligible and occur with a typical frequency of about one such interaction per several thousand particles transmitted through a thin foil. The following conclusions can now be made:

1. A charged particle traversing a foil will have numerous soft interactions with scattering centers in the absorber that are random and independent from one another. These interactions result in small individual deflections from the incident direction as well as in a small cumulative scattering angle  $\Theta$ .
2. One in several 1000 particles of the particle beam traversing a foil will have a hard interaction (close encounter) with a scattering center resulting in a large-angle deflection. Because of the very small probability for a hard collision, only one such large angle deflection can occur to a given charged particle. All large-angle deflections are therefore attributed to one single-scattering event for a given charged particle.
3. The angular distribution of charged particles traversing a foil thus has three regions:
  - a. Small angle  $\Theta$  region governed by a Gaussian distribution resulting from Molière multiple scattering.
  - b. Large angle single-scatter region produced by a small fraction of particles striking the foil and resulting from single hard collisions between a charged particle and a scattering center.
  - c. Intermediate region between the multiple scatter small-angle region and the single-scatter large-scattering angle region referred to as the region of *plural scattering*. The plural scattering distribution enables the transition from the multiple scattering region into the single scattering region.

The mean square angle  $\overline{\theta^2}$  for single scattering derived in Sect. 2.6.5 also plays a role in determining the mean square angle  $\overline{\Theta^2}$  which governs the Gaussian distribution in Molière multiple scattering distribution, as shown in Sect 2.7.1.

### 2.7.1 Mean Square Scattering Angle for Multiple Scattering

The thicker is the absorber and the larger is its atomic number  $Z$ , the greater is the likelihood that the incident particle will undergo several single scattering events. For a sufficiently thick absorber the mean number of successive encounters rises to a value that permits a statistical treatment of the process. Generally, 20 collisions are deemed sufficient and we then speak of multiple Coulomb scattering that is characterized by a large succession of small angle deflections symmetrically distributed about the incident particle direction.

The mean square angle for multiple Coulomb scattering  $\overline{\Theta^2}$  is calculated from the mean square angle for single scattering  $\overline{\theta^2}$  (2.128) with the help of the *central limit theorem* that states the following:

*For a large number  $N$  of experiments that measure some stochastic variable  $X$ , the probability distribution of the average of all measurements is Gaussian and is centered at  $\overline{X}$  with a standard deviation  $1/\sqrt{N}$  times the standard deviation of the probability density of  $X$ .*

Since the successive single scattering collisions in the absorber are independent events, the central limit theorem shows that for a large number  $n > 20$  of such collisions the distribution in angle will be Gaussian around the forward direction with a mean square scattering angle  $\overline{\Theta^2}$  given as

$$\overline{\Theta^2} = n\overline{\theta^2}, \quad (2.131)$$

where

$\overline{\theta^2}$  is the mean square scattering angle for single scattering given in (2.128),  
 $n$  is the number of scattering events calculated as follows

$$n = \frac{N_a}{V} \sigma t = \rho \frac{N_A}{A} \sigma t \approx \pi \rho \frac{N_A}{A} \frac{D^2}{\theta_{\min}^2} t \quad (2.132)$$

where we inserted the expression of (2.125) for the cross section and

$N_a/V$  is number of atoms per volume equal to  $\rho N_A/A$ ,  
 $\sigma$  is the total cross section for a single scattering event given in (2.124) and (2.125),  
 $t$  is thickness of the absorber,  
 $\rho$  is density of the absorber,  
 $N_A$  is the Avogadro number,  
 $A$  is the atomic mass number of the absorber.

Incorporating the expression for the mean square angle for single scattering  $\overline{\theta^2}$  from (2.128) into (2.131) and using (2.132) for the number of scattering events, the mean square angle for multiple scattering  $\overline{\Theta^2}$  can be written as

$$\overline{\Theta^2} = \rho \frac{N_A}{A} \sigma t \theta_{\min}^2 \left\{ \ln \left( 1 + \frac{\theta_{\max}^2}{\theta_{\min}^2} \right) - \frac{1}{1 + \theta_{\min}^2/\theta_{\max}^2} \right\}, \quad (2.133)$$

where  $\theta_{\min}$  and  $\theta_{\max}$  are the minimum and maximum scattering angles, respectively, defined in Sect. 2.6.3, and  $D$  is the characteristic scattering distance for a particular scattering event, defined in Sec. 2.6.2.

Since  $\theta_{\max} \gg \theta_{\min}$  holds in general, we can simplify (2.133) for heavy charged particle scattering on nuclei of an absorber by inserting (2.125) for the total cross section  $\sigma$  with (2.113) for the characteristic scattering distance  $D$  and (2.130) for  $\overline{\theta^2}$  to get

$$\begin{aligned} \overline{\Theta^2} &= n\overline{\theta^2} = 4 \left( \rho \frac{N_A}{A} \sigma t \right) \theta_{\min}^2 \ln[183Z^{-1/3}] = 4\pi \rho \frac{N_A}{A} D^2 t \ln[183Z^{-1/3}] \\ &= 4\pi \rho \frac{N_A}{A} \left( \frac{2zZe^2}{4\pi\epsilon_0 p v} \right)^2 \{ \ln[183Z^{-1/3}] \} t. \end{aligned} \quad (2.134)$$

Similarly, for electrons scattered on absorber atoms (nuclei and orbital electrons) we simplify (2.133) by inserting (2.125) for the total cross section  $\sigma$  with (2.118) for the characteristic scattering distance  $D$  and (2.130) for  $\overline{\theta^2}$  to get

$$\begin{aligned}\overline{\Theta^2} &= n\overline{\theta^2} = \left(\rho \frac{N_A}{A} \sigma t\right) 4\theta_{\min}^2 \ln[183Z^{-1/3}] \\ &= 16\pi\rho \frac{N_A r_e^2 Z(Z+1)}{A\gamma^2\beta^4} \{\ln[183Z^{-1/3}]\}t = \frac{4\pi\rho}{\alpha X_0}t,\end{aligned}\quad (2.135)$$

where  $X_0$  is defined as the radiation length and discussed in Sect. 2.7.2.

From (2.135) we can express the change in the mean square scattering angle  $\overline{\Theta^2}$  with propagation distance  $t$  in the foil as

$$\frac{d\overline{\Theta^2}}{dt} = 16\pi\rho \frac{N_A r_e^2 Z(Z+1)}{A\gamma^2\beta^4} \ln[183Z^{-1/3}] = \frac{4\pi\rho}{\alpha X_0}.\quad (2.136)$$

As shown in (2.134) and (2.135), the mean square scattering angle  $\overline{\Theta^2}$  for multiple scattering increases linearly with the foil thickness  $t$  but, as long as the foil thickness is not excessive, the angular distribution of transmitted particles will remain Gaussian and forward peaked.

### 2.7.2 Radiation Length

The expressions for the mean square scattering angle  $\overline{\Theta^2}$  of (2.135) and (2.136) can be expressed in terms of a distance parameter called the radiation length  $X_0$ . This parameter serves as a unit of length, depends on the mass of the charged particle as well as on the atomic number of the absorbing material, and is defined as the mean distance a relativistic charged particle travels in an absorbing medium while its energy, due to radiation loss, decreases to  $1/e$  ( $\sim 36.8\%$ ) of its initial value.  $X_0$  is also defined as  $7/9$  of the mean free path for pair production by a high energy photon in the absorber.

The radiation length  $X_0$ , which usually refers to electrons, is expressed in square centimeters per gram as follows

$$\begin{aligned}\frac{1}{X_0} &= 4\alpha \frac{N_A}{A} Z(Z+1)r_e^2 \ln(183Z^{-1/3}) \\ &= 1.4 \times 10^{-3} (\text{cm}^2/\text{mol}) \frac{Z(Z+1)}{A} \ln(183Z^{-1/3}),\end{aligned}\quad (2.137)$$

where

- $\alpha$  is the fine structure constant (1/137),
- $N_A$  is the Avogadro number ( $6.022 \times 10^{23}/\text{mol}$ ),
- $Z$  is the atomic number of the absorber,
- $r_e$  is the classical electron radius (2.818 fm).

For electrons, values of radiation length  $X_0$  calculated from (2.137) are  $24 \text{ g/cm}^2$  (9 cm) in aluminum;  $10.2 \text{ g/cm}^2$  (1.1 cm) in copper; and  $5.8 \text{ g/cm}^2$  (0.51 cm) in lead.

### 2.7.3 Mass Scattering Power

As shown in (2.133), the mean square scattering angle for multiple scattering  $\overline{\Theta^2}$  increases linearly with the absorber thickness  $t$ . A mass scattering power  $T/\rho$  can thus be defined for electrons:

1. Either as the mean square angle for multiple scattering  $\overline{\Theta^2}$  per mass thickness  $\rho t$ .
2. Or the increase in the mean square angle  $\overline{\Theta^2}$  per unit mass thickness  $\rho t$ , in analogy with the mass stopping power.

The mass scattering power ( $T/\rho$ ) is thus expressed as follows

$$\frac{T}{\rho} = \frac{\overline{\Theta^2}}{\rho t} = \frac{d\overline{\Theta^2}}{d(\rho t)} = \frac{N_A}{A} \sigma \theta_{\min}^2 \left\{ \ln \left( 1 + \frac{\theta_{\max}^2}{\theta_{\min}^2} \right) - \frac{1}{1 + \theta_{\min}^2/\theta_{\max}^2} \right\} \quad (2.138)$$

and this result, after inserting (2.125) for the total cross section  $\sigma$ , is usually given as follows (ICRU #35)

$$\frac{T}{\rho} = \pi \frac{N_A}{A} D^2 \left\{ \ln \left( 1 + \frac{\theta_{\max}^2}{\theta_{\min}^2} \right) - 1 + \left[ 1 + \frac{\theta_{\max}^2}{\theta_{\min}^2} \right]^{-1} \right\}, \quad (2.139)$$

with  $D$ , the effective characteristic scattering distance, discussed in Sect. 2.6.2 for various scattering interactions.

### 2.7.4 Mass Scattering Power for Electrons

The mass scattering power  $T/\rho$  for electrons is determined from the general relationship of (2.139) by inserting (2.118) for the characteristic distance  $D$  in electron scattering with nuclei and orbital electrons of the absorber foil to get

$$\frac{T}{\rho} = 2\pi r_e^2 \frac{N_A Z(Z+1)}{A} \frac{\sqrt{1-\beta^2}}{\beta^2} \left\{ \ln \left( 1 + \frac{\theta_{\max}^2}{\theta_{\min}^2} \right) - 1 + \left[ 1 + \frac{\theta_{\max}^2}{\theta_{\min}^2} \right]^{-1} \right\}. \quad (2.140)$$

The term  $(\sqrt{1-\beta^2})/\beta^2$  in (2.118) for  $D$  can be expressed in terms of the electron kinetic energy  $E_K$  and electron rest energy  $E_0 = m_e c^2$ . We first define the ratio  $E_K/(m_e c^2)$  as  $\tau$  and then use the standard relativistic relationship for the total energy of the electron, i.e.,

$$m_e c^2 + E_K = \frac{m_e c^2}{\sqrt{1-\beta^2}} \quad (2.141)$$

to obtain

$$\sqrt{1-\beta^2} = \frac{1}{1+\tau} \quad (2.142)$$

and

$$\beta^2 = \frac{\tau(2 + \tau)}{(1 + \tau)^2}, \quad (2.143)$$

resulting in the following expression for the term  $\frac{\sqrt{1 - \beta^2}}{\beta^2}$

$$\frac{\sqrt{1 - \beta^2}}{\beta^2} = \frac{1 + \tau}{\tau(2 + \tau)}. \quad (2.144)$$

The mass scattering power  $T/\rho$  of (2.139) for electron may then be expressed as follows

$$\frac{T}{\rho} = 4\pi \frac{N_A}{A} r_e^2 Z(Z + 1) \left[ \frac{1 + \tau}{\tau(2 + \tau)} \right]^2 \left\{ \ln \left( 1 + \frac{\theta_{\max}^2}{\theta_{\min}^2} \right) - 1 + \left[ 1 + \frac{\theta_{\max}^2}{\theta_{\min}^2} \right]^{-1} \right\}. \quad (2.145)$$

In (2.145),  $\theta_{\max}$  is the cutoff angle resulting from the finite size of the nucleus. In (2.122), the cutoff angle  $\theta_{\max}$  was given by the ratio of the reduced de Broglie wavelength of the electron  $\hbar/p_e$  to the nuclear radius  $R$  given in (1.26) as  $R = R_0 \sqrt[3]{A}$  with  $R_0 = 1.25$  fm the nuclear radius constant and  $A$  the nucleon number or atomic mass number. The electron momentum  $p_e$  using (1.60) and (2.142) can be expressed as

$$\begin{aligned} p_e &= \frac{1}{c} \sqrt{E^2 - E_0^2} = \frac{1}{c} \sqrt{E_K(E_K + 2E_0)} \\ &= \frac{1}{c} E_0 \sqrt{\frac{1}{1 - \beta^2} - 1} = \frac{E_0 \beta}{c \sqrt{1 - \beta^2}} = \frac{E_0 \beta (1 + \tau)}{c} \end{aligned} \quad (2.146)$$

giving the following expression for  $\theta_{\max}$

$$\begin{aligned} \theta_{\max} &= \frac{\hbar}{p_e R} = \frac{\hbar c A^{-1/3}}{R_0 \sqrt{E_K(E_K + 2E_0)}} \\ &= \frac{\hbar c A^{-1/3}}{E_0 \beta (1 + \tau) R_0} \approx \frac{\alpha a_0 A^{-1/3}}{\beta (1 + \tau) R_0} \approx \frac{309 A^{-1/3}}{\beta (1 + \tau)}, \end{aligned} \quad (2.147)$$

with

- $\beta$  electron velocity normalized to  $c$ , the speed of light in vacuum,
- $A$  atomic mass number of the absorber,
- $\tau$  electron kinetic energy normalized to electron rest mass energy  $E_0$ ,
- $E_K$  electron kinetic energy.

The screening angle  $\theta_{\min}$  results from the screening of the nucleus by the atomic orbital electrons and is expressed in (2.121) by the ratio of the reduced de Broglie wavelength of the electron  $\hbar/p_e$  [given in (2.71)] to the Thomas–Fermi atomic radius  $a_{\text{TF}}$  given in (2.49) as  $a_{\text{TF}} \approx a_0 Z^{-1/3}$ , with  $a_0$  the Bohr radius constant of (3.4) and  $Z$  the atomic number of the absorber. Recognizing that  $\hbar c / (E_0 a_0) = \alpha$ , the minimum scattering angle, also known

as the *screening angle*,  $\theta_{\min}$  can be expressed as

$$\theta_{\min} = \frac{\hbar}{p_e a_{\text{TF}}} = \frac{\hbar c Z^{1/3}}{E_0 \beta (1 + \tau) a_0} = \frac{\alpha Z^{1/3}}{\beta (1 + \tau)} = \frac{Z^{1/3}}{137 \beta (1 + \tau)} \quad (2.148)$$

with

- $\beta$  electron velocity normalized to speed of light in vacuum  $c$ ,
- $Z$  atomic number of the absorber,
- $\tau$  electron kinetic energy normalized to electron rest mass energy, i.e.,  $\tau = E_K / (m_e c^2)$ , and
- $\alpha$  fine structure constant ( $1/137$ ).

Similarly to the expression in (2.74) and (2.123), the ratio  $\theta_{\max}/\theta_{\min}$  is now given by a simple expression independent of electron rest energy  $E_0$  and kinetic energy  $E_K$

$$\frac{\theta_{\max}}{\theta_{\min}} = \frac{309 \times 137 A^{-1/3}}{Z^{1/3}} \approx \frac{0.423 \times 10^5}{\sqrt[3]{AZ}}, \quad (2.149)$$

and ranges from  $\theta_{\max}/\theta_{\min} \approx 0.42 \times 10^5$  for hydrogen to  $\theta_{\max}/\theta_{\min} \approx 1500$  for uranium-235.

Two features of the mass scattering power  $T/\rho$  can be identified:

1.  $(T/\rho)$  is roughly proportional to  $Z$ . This follows from the  $Z(Z + 1)/A$  dependence recognizing that  $A \approx 2Z$  to obtain  $(T/\rho) \propto Z$ .
2.  $(T/\rho)$  for large electron kinetic energies  $E_K$  where  $\tau \gg 1$  is proportional to  $1/E_K^2$ . This follows from  $(1 + \tau)^2 / \{\tau(2 + \tau)\}^2 \approx 1/\tau^2$  for  $\tau \gg 1$ .

A plot of the mass scattering power  $(T/\rho)$  for electrons in various materials of interest in medical physics in the electron kinetic energy range from 1 keV to 1000 MeV is given in Fig. 2.13. The mass scattering power  $(T/\rho)$  consists of two components: the electron–nucleus (e–N) scattering and the electron–orbital electron (e–e) scattering.

### 2.7.5 Fermi-Eyges Pencil Beam Model for Electrons

Fermi in his study of cosmic radiation derived an analytical solution to the transport equation for energetic charged particles traversing thin foils. He used Molière’s small angle multiple scattering approximation and assumed that the energetic cosmic particles lost no energy in the thin foils he used in his experiments. Eyges extended Fermi’s work to electron pencil beams traversing absorbing media and accounted for electron energy loss as well as for electron transport through heterogeneous absorbers.

As shown in Fig. 2.14, electrons moving in a pencil beam along the  $z$  axis (applicator axis) of a Cartesian coordinate system strike the absorber at the origin  $(0,0,0)$  of the coordinate system and undergo multiple scattering interactions as they penetrate into the absorber. After traversing a given thickness of the absorber, each electron emerges in a direction defined by angles

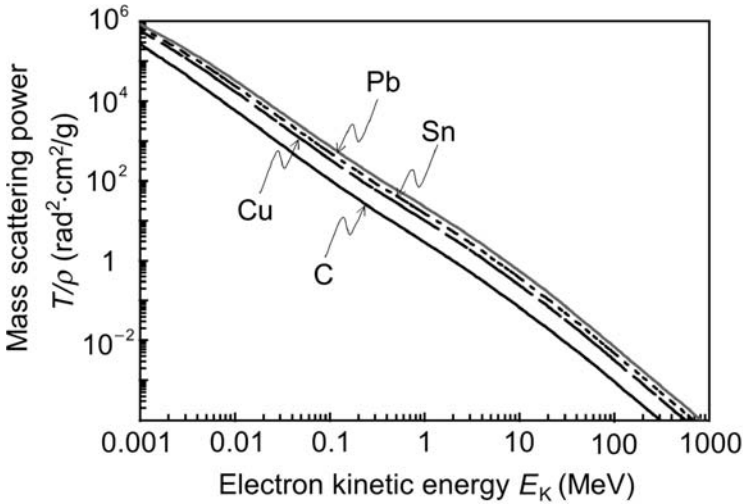


**Fig. 2.13.** Mass scattering power ( $T/\rho$ ) against electron kinetic energy  $E_K$  for various materials of interest in medical physics

$\Theta$  and  $\Phi$ . The projections of the polar angle  $\Theta$  onto the  $(x,z)$  and  $(y,z)$  planes are  $\Theta_x$  and  $\Theta_y$ , respectively.

The Fermi-Eyges solution to the transport equation gives the probability  $P(x, z)dx$  of finding an electron at depth  $z$  in the absorber with a displacement from the original  $z$  direction between  $x$  and  $x + dx$  on the abscissa and the probability  $P(y, z)dy$  of finding the electron between  $y$  and  $y + dy$  on the ordinate. The two probability density functions  $P(x, z)dx$  and  $P(y, z)dy$  are given as follows (see Sect. 1.30)

$$P(x, z)dx = \frac{1}{\sigma(z)\sqrt{2\pi}} e^{-\frac{x^2}{2[\sigma(z)]^2}} dx \tag{2.150}$$

and

$$P(y, z)dy = \frac{1}{\sigma(z)\sqrt{2\pi}} e^{-\frac{y^2}{2[\sigma(z)]^2}} dy, \tag{2.151}$$

with  $\sigma(z)$  representing the standard deviation of the mean as a measure of the width of the distribution at depth  $z$ . According to the Fermi-Eyges theory the variance  $v(z)$  which by definition is the square of the standard deviation  $\sigma(z)$  is expressed as

$$v(z) = [\sigma(z)]^2 = \frac{1}{2} \int_0^z T(z') [z - z']^2 dz', \tag{2.152}$$

where  $T(z')$  is the linear scattering power of the absorber at depth  $z'$ , evaluated for the mean electron energy at depth  $z'$ . The scattering power  $T$  was discussed in Sect. 2.7.3 and shown to be proportional to the mean square scattering angle  $\Theta^2$  in (2.138).

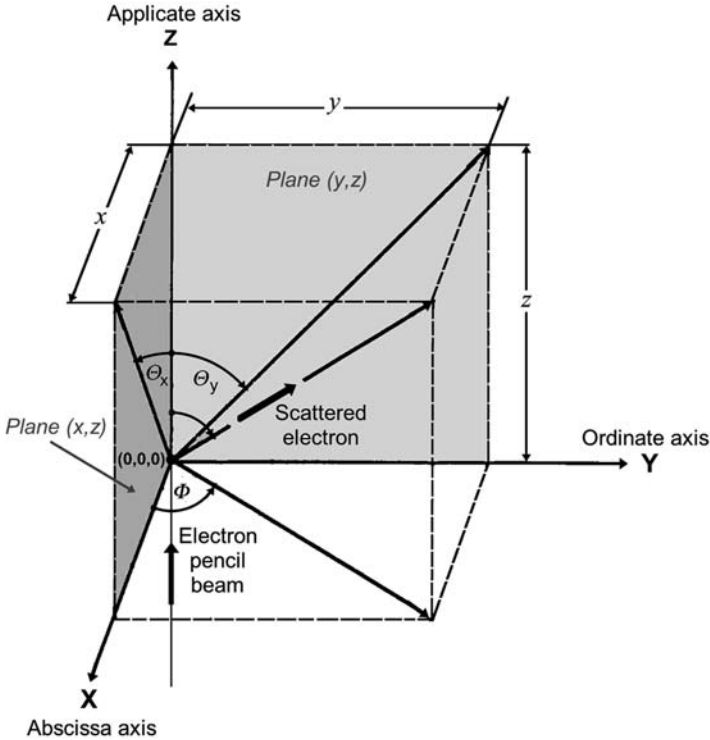


**Fig. 2.14.** Electrons in a pencil beam moving along applicate ( $z$ ) axis of a Cartesian coordinate system strike an absorber at the origin of the coordinate system and undergo multiple scattering interactions as they penetrate into the absorber. After traversing a given thickness of the absorber, each electron emerges in a direction defined by angles  $\theta$  and  $\phi$

In general, the combined probability  $P(x, y, z)dxdy$  is a product of the two probability density functions,  $P(x, z)dx$  of (2.150) and  $P(y, z)dy$  of (2.151), expressed as follows

$$P(x, y, z)dxdy = [P(x, z)dx] \times [P(y, z)dy] = \frac{1}{2\pi[\sigma(z)]^2} e^{-\frac{x^2+y^2}{2[\sigma(z)]^2}} dxdy. \tag{2.153}$$

From Fig. 2.14 we get the following relationships among angles  $\theta$ ,  $\theta_x$ ,  $\theta_y$ , and  $\phi$  and Cartesian coordinates  $x$ ,  $y$ , and  $z$

$$\tan \theta = \frac{x / \cos \phi}{z} = \frac{x / \sin \phi}{z}, \tag{2.154}$$

$$\tan \theta_x = \frac{x}{z} = \tan \theta \cos \phi, \tag{2.155}$$

$$\tan \theta_y = \frac{y}{z} = \tan \theta \sin \phi, \tag{2.156}$$

$$\tan^2 \theta = \tan^2 \theta_x + \tan^2 \theta_y. \tag{2.157}$$

In the small angle approximation where  $\sin \Theta \approx \Theta$ ,  $\cos \Theta \approx 1$ , and  $\tan \Theta \approx \Theta$ , the relationship of (2.157) connecting  $\Theta$ ,  $\Theta_x$ , and  $\Theta_y$  simplifies to read

$$\Theta^2 = \Theta_x^2 + \Theta_y^2 \quad (2.158)$$

and, since the scattering events are symmetrical about the initial direction  $z$ , the following relationships also apply

$$\overline{\Theta_x^2} = \overline{\Theta_y^2} = \frac{1}{2}\overline{\Theta^2}. \quad (2.159)$$

The final polar angle  $\Theta$  following multiple scattering events cannot be determined by a simple addition of the polar angles for the individual scattering events because of the  $\Phi$  component which is present in each single scattering event. The projections  $\Theta_x$  and  $\Theta_y$ , however, are additive and this then allows us to apply the central limit theorem stated in Sect. 2.7.1. For the  $(x,z)$  plane we define  $P(x, \Theta_x, z)d\Theta_x$  as the probability that an electron, after traversing an absorber thickness  $dz$ , will be deflected through an angle, the projection of which onto the  $(x,z)$  plane will be between  $\Theta_x$  and  $\Theta_x + d\Theta_x$ . Similarly, for the  $(y,z)$  plane we define  $P(y, \Theta_y, z)d\Theta_y$  as the probability that an electron, after traversing an absorber thickness  $dz$ , will be deflected through an angle, the projection of which onto the  $(y,z)$  plane will be between  $\Theta_y$  and  $\Theta_y + d\Theta_y$ .

The two probability functions  $P(x, \Theta_x, z)$  and  $P(y, \Theta_y, z)$  are Gaussian functions expressed as

$$P(x, \Theta_x, z) = \frac{1}{\sqrt{2\pi\overline{\Theta_x^2}}} e^{-\frac{\Theta_x^2}{2\overline{\Theta_x^2}}} = \frac{1}{\sqrt{\pi\overline{\Theta^2}}} e^{-\frac{\Theta_x^2}{\overline{\Theta^2}}} \quad (2.160)$$

and

$$P(y, \Theta_y, z) = \frac{1}{\sqrt{2\pi\overline{\Theta_y^2}}} e^{-\frac{\Theta_y^2}{2\overline{\Theta_y^2}}} = \frac{1}{\sqrt{\pi\overline{\Theta^2}}} e^{-\frac{\Theta_y^2}{\overline{\Theta^2}}}, \quad (2.161)$$

where we used (2.159) to modify the two original Gaussian distributions.

Similarly to (2.153), the combined probability  $P(x, \Theta_x, y, \Theta_y, z)$  is given as the product of the two probability functions  $P(x, \Theta_x, z)$  and  $P(y, \Theta_y, z)$  to give

$$\begin{aligned} P(x, \Theta_x, y, \Theta_y, z) &= P(x, \Theta_x, z) \times P(y, \Theta_y, z) \\ &= \frac{1}{\sqrt{\pi\overline{\Theta^2}}} e^{-\frac{\Theta_x^2}{\overline{\Theta^2}}} \frac{1}{\sqrt{\pi\overline{\Theta^2}}} e^{-\frac{\Theta_y^2}{\overline{\Theta^2}}} = \frac{1}{\pi\overline{\Theta^2}} e^{-\frac{\Theta^2}{\overline{\Theta^2}}}, \end{aligned} \quad (2.162)$$

after we use (2.158) for the sum of  $\Theta_x^2$  and  $\Theta_y^2$ .

The discussion of the Thomson model of the atom in Sect. 2.2.1 made use of (2.162) when in (2.2) we estimated  $N(\Theta)d\Theta$ , the number of  $\alpha$  particles that are scattered on gold nuclei within the angular range  $\Theta$  to  $\Theta + d\Theta$ , with  $N_0$  representing the number of  $\alpha$  particles striking, and passing through, the gold foil. The fractional number of  $\alpha$  particles scattered into the angular range

$\Theta$  to  $\Theta + d\Theta$  is expressed as follows

$$\begin{aligned} \frac{N(\Theta)d\Theta}{N_0} &= P(x, \Theta_x, y, \Theta_y, z)d\Omega = 2\pi P(x, \Theta_x, y, \Theta_y, z) \sin \Theta d\Theta \\ &\approx 2\pi\Theta \frac{1}{\pi\Theta^2} e^{-\frac{\Theta^2}{\bar{\Theta}^2}} d\Theta = \frac{2\Theta}{\Theta^2} e^{-\frac{\Theta^2}{\bar{\Theta}^2}} d\Theta = e^{-\frac{\Theta^2}{\bar{\Theta}^2}} d\frac{\Theta^2}{\bar{\Theta}^2}, \end{aligned} \quad (2.163)$$

where we used the small angle approximation  $\sin \Theta \approx \Theta$ .

An integration of (2.163) over  $\Theta$  from 0 to  $\pi$  results in 1, since  $\bar{\Theta}^2$ , the mean square scattering angle for multiple scattering, is very small. The  $\Theta$  angular distribution is strongly peaked in the forward ( $z$ ) direction of the incident pencil electron beam, with  $\bar{\Theta}$ , the mean scattering angle  $\Theta$ , equal to 0 and  $\sqrt{\bar{\Theta}^2}$ , the root mean square angle for multiple scattering of the order of  $1^\circ$ .

### 2.7.6 Dose Distribution for Pencil Electron Beam

The dose distribution for a pencil electron beam in absorbing medium is related to the distribution function given by the Fermi-Eyges solution to the Fermi electron transport equation that in three dimensions is expressed as follows

$$\frac{\partial P}{\partial z} = -\Theta_x \frac{\partial P}{\partial \Theta_x} - \Theta_y \frac{\partial P}{\partial \Theta_y} + \frac{T(x, y, z)}{4} \left( \frac{\partial^2 P}{\partial \Theta_x^2} + \frac{\partial^2 P}{\partial \Theta_y^2} \right), \quad (2.164)$$

with  $T(x, y, z)$  the linear scattering power of the absorber and the probability function  $P$  given as a product of two Gaussian probability functions

$$P = P(x, \Theta_x, y, \Theta_y, z) = P(x, \Theta_x, z) \times P(y, \Theta_y, z) \quad (2.165)$$

The Fermi-Eyges theory predicts that the dose distribution in the absorber, in a plane perpendicular to the incident direction of the initial pencil electron beam, is represented by a Gaussian distribution. The theory also predicts that the spatial spread of the electron beam in the absorber is an increasing function of depth in the absorber irrespective of the depth. However, experiments show that the spatial spread indeed increases with depth from the absorber surface to about a depth close to  $2/3$  of the practical electron range, but at larger depths the spatial spread saturates, then decreases, and vanishes at depths greater than the range of electrons in the absorber.

The Fermi-Eyges theory considers only the small angle multiple Coulomb scattering and assumes that the energy of the electron, as it moves through the phantom, is dependent only on depth and that no electrons are absorbed in the scattering medium. This is certainly an improvement over the Fermi assumption of no energy loss of charged particles in the absorber; however, neglecting the electron absorption in the absorber causes significant discrepancy between measurement and Fermi-Eyges theory at depths close to the electron range.

### 2.7.7 Determination of Electron beam Kinetic Energy from Measured Mass Scattering Power

The plot of  $(T/\rho)$  against electron kinetic energy  $E_K$  for kinetic energies in the megavoltage energy range (Fig. 2.13) is essentially linear on a log-log plot resulting in the  $(T/\rho) \propto 1/E_K^2$  dependence. The steady  $1/E_K^2$  drop of  $(T/\rho)$  as a function of increasing  $E_K$  suggests a relatively simple means for electron kinetic energy determination from a measurement of the mass scattering power  $(T/\rho)$  in a given medium.

The propagation of an electron pencil beam in an absorber is described by a distribution function that is given by the Fermi-Eyges solution to the Fermi differential transport equation. The Fermi-Eyges theory predicts that the dose distribution in a medium on a plane perpendicular to the incident direction of the pencil electron beam is given by a Gaussian distribution with a spatial spread proportional to the variance of the Gaussian distribution.

Equation (2.152) shows that the variance  $[\sigma(z)]^2$  of the Gaussian distribution is related to the scattering power  $T(z)$  at depth  $z$ . In situations where the scattering power  $T(z)$  of the absorber is constant in the absorber thickness  $z$  (for example, in measurements of spatial spread in air layers  $z$  much thinner than the range of electrons in air), (2.152) can be simplified to read

$$\begin{aligned} [\sigma(z)]^2 &= \frac{1}{2} \int_0^z T(z') [z - z']^2 dz' = \frac{1}{2} T(z) \int_0^z [z - z']^2 dz' \\ &= \frac{1}{2} T(z) \int_0^z [z^2 - 2zz' + (z')^2] dz' = \frac{1}{6} z^3 T(z). \end{aligned} \quad (2.166)$$

In deriving (2.166) the following assumptions are made:

1. Only small angle scattering events are considered.
2. The air layer  $z$  is much smaller than the electron range in air.
3. Secondary electrons, set in motion by the electron incident pencil beam, are ignored.
4. The bremsstrahlung contamination of the electron pencil beam is ignored.

Function  $[\sigma(z)]^2$  given in (2.166) is a linear function of  $z^3$  with the slope proportional to the mass scattering power  $(T/\rho)$ , which in turn is a function of electron beam kinetic energy  $E_K$  through function  $\tau$ , as given in (2.146). Thus, from a measurement of  $[\sigma(z)]^2$ , the spatial spread of an electron pencil beam in air, at several distances  $z$  from the pencil beam origin, one first determines  $(T/\rho)$  through (2.166) and then determines the electron beam kinetic energy  $E_K$  with data tabulated for air or data calculated for air from (2.146).